This is to certify that the
thesis entitled

Quasi-Three Dimensional Woven Composites

presented by

Kirit Keith Rosario

has been accepted towards fulfillment
of the requirements for the

M.S. degree in Mechanical Engineering

Major Professor's Signature

8/4/08

Date

QUASI-THREE-DIMENSIONAL WOVEN COMPOSITES

By

Kirit Keith Rosario

A THESIS

Submitted to
Michigan State University
In partial fulfillment of the requirements
for the degree of

MASTER OF SCIENCE

Department of Mechanical Engineering

2008

ABSTRACT

QUASI-THREE-DIMENSIONAL WOVEN COMPOSITES

By

Kirit Keith Rosario

The phenomenon of delamination hinders the unreserved use of composite materials in strategic applications especially those which might involve fatigue or impact loading. This thesis explores the effect of inter-laminar three-dimensional (Quasi-three-dimensional) fabric weaving on the structural, energy absorption and damage resistance properties of glass-epoxy composites in a low-velocity penetrative impact event, through experimental studies. Traditionally used laminated and two-dimensionally woven composites are used as references for comparison of performance. It was found that quasi-three-dimensional composites are viable alternatives to traditional composite systems where energy absorption or damage resistance is of greater importance.

To the love of my life, Rahael

ACKNOWLEDGEMENTS

I would like to acknowledge, and am very grateful for, the support, guidance, active participation and fatherly concern of my academic advisor Dr. Dahsin Liu, without whom this thesis would not have been possible.

I am grateful to Dr. Alfred Loos for time provided to me on his equipment, and to TARDEC, Warren MI, for the use of their impact testing machine.

I would also like to thank my co-workers Elias Shakour, Goijing Li, Jeffery Fuller and Shawn Klann for their extensive assistance, advice and companionship during this study.

TABLE OF CONTENTS

LIST OF TABLES

LIST OF FIGURES

KEY TO SYMBOLS AND ABBREVIATIONS

L	=	laminated
2D	=	2-dimensionally woven
Q3D	=	2-harness quasi 3-dimensionally woven
Q3DO3	=	3-harness quasi 3-dimensionally woven with offset
Q3DO5	=	5-harness quasi 3-dimensionally woven with offset
v_i	=	initial tup velocity
t_b	=	time period between voltage spikes of velocity sensor blades
s	=	distance between leading edges of flag blades
F(t)	=	instantaneous impact force
a(t)	=	instantaneous acceleration of drop weight
m	=	mass of drop weight
v(t)	=	instantaneous velocity of drop weight
$\delta(t)$	=	instantaneous deflection of specimen
CAI	=	compression after impact
v_f	=	fiber volume fraction
w_{dry}	=	weight of dry specimen
w_{wet}	=	weight of specimen submerged in water
ρ_w	=	density of water at experimental conditions
ρ_c	=	density of composite
ρ_f	=	density of glass fiber
ρ_r	=	density of epoxy resin
SEA	=	specific energy absorption

CHAPTER 1

Introduction

1.1 Background and Literature Review

Fiber-reinforced composite materials have already made their mark in today's engineering world as materials to be reckoned with, owing to their high stiffness and high strength with low density. In addition to these, they can have favorable properties of being orthotropic which enable them to be tailored to specific applications where stiffness, strength or other physical properties are required in only particular directions in a component or structure. Their method of preparation from soft, pliable sheets and liquid resins, or pliable pre-preg lend them to be used successfully in the manufacture of parts with complicated geometries with greater ease than would be possible with conventional materials and machining processes.

Fiber-reinforced composite materials have, however, been known to have some undesirable properties which have held back their unreserved use in critical applications. One of the biggest of these problems is that of delamination. Delamination is the phenomenon where the plies that build up the composite material separate from each other due to breakage of interfacial matrix material. This can be due to shear or tensile stresses that build up in these regions due to a variety of loading conditions, such as bending and impact events. It seems to be commonly accepted that the cause for delamination in composite panels is a mismatch in the bending stiffness of adjacent layers, causing the matrix material

at the interface to shear when the composite panels are loaded with transverse impact forces [1,2,3,4,5,6,7]. Delamination, which can often go unnoticed in thicker, less transparent materials, reduces the structural properties of the material, especially its compressive properties [1]. Delamination can be caused by low-velocity impacts to the material from routine incidents during operation. Once delamination is initialized, it has been known to propagate itself with further component loading, reducing the components strength and structural integrity. An understanding of the possible steps that can be taken to prevent, or at least to reduce the effects of delamination, without sacrificing much of the composites' desirable properties will prove useful. When the material is used as a protective layer to withstand penetrative impact, then the desired property would be high impact energy absorption, whereas when energy absorption is not the main criterion, resistance to damage propagation is of greater importance. These two do not always go hand in hand, and sometimes one is gained at the loss of the other. A good balance between the two is most desirable for a versatile material which can serve in a variety of operating conditions.

There are various methods that have been suggested in order to tackle the problem of delamination due to impact. It can be done either by reducing the inter-laminar stresses (by reducing inter-ply layup angles or reducing ply thickness) or by increasing the inter-laminar strength (by means of stitching, Z-pinning, etc.) [1,3,8,9,10]. Various authors have worked on trying to characterize unidirectional laminated and two-dimensionally woven composite materials, with a focus on their microscopic fiber geometries, in an effort to better improve their

damage and post-damage residual properties. They link properties like stiffness, fiber volume fraction and impact energy absorption to weave-level features like harness number, inter-layer integration, fiber angle and cell size [1,3,8,11,12]. Simulation and analysis based studies have focused on the properties of just fabric [11,13,14] and fabric-matrix systems [15]. Some papers have discussed the inherent advantages of three-dimensionally woven fabrics [9,10,16-18], but they are mostly directed towards through-thickness 'stitched' geometries, Z-pinning or braided geometries.

There are a few authors who have tried to characterize angle interlocked three-dimensionally woven fabrics (hereafter referred to as quasi-three-dimensional), but only to the extent of formability and pliability [17]. However, detailed work on the impact properties of inter-laminar, three-dimensionally integrated fabrics seems limited [2,5] and this issue seems complex enough to warrant deeper investigation, while considering in addition, the post-impact residual strengths of materials produced from these weaves. It is also seen from the review paper by A.P. Mouritz *et al* [19] that there is a large amount of contradictions in the findings of different studies in the area of three-dimensionally integrated composites. Harness effects on the quasi-three-dimensional weaves too require some attention as increase in harness number has the potential to more closely replicate the performance of traditional composite material systems. Stitched satin weaves with high harness performed better in impact energy absorption than plain weaves [18]. Damage to fibers during the weaving of three-dimensional woven fabrics has been investigated in

order to refine the weaving procedure to produce more accurate specimens [20,21].

Many studies have been carried out to understand the damage processes involved in energy absorption during an impact event [1,2,3,5,7,11]. The most widely accepted method for impact characterization seems to be the use of an instrumented drop-weight tester. By impacting specimens at various impact energy levels, the progressive damage modes are suggested [1,2,5,7,18,22]. The damage processes were described in terms of fiber breakage, fiber pull-out, matrix cracking, and delamination. It has been reported [1] that the pivotal point in a damage event is perforation, although the perforation itself causes little degradation of properties of the composite [22]. Several papers have looked into the effects of the various parameters involved in the impact testing like impact velocity, boundary conditions and impactor size and shape [1,23-25]. A variety of methods of destructive and non-destructive testing have been used in order to visualize structures and damage patterns within the samples, like C-scan, edge replication, ultrasonics and use of light table [7,12,18,26]. In order to characterize the post-impact residual properties, compressive, tensile and fatigue loadings have been used on impacted specimens [1,4,10,16,22,23,27]. It appears that compressive strength is regarded as the most important of these as it is the most sensitive to impact damage [4,16,22,23].

1.2 Statement of Problem and Goal of Thesis

It is accepted that delamination is a prominent and undesired occurance in conventional forms of fiber-reinforced composite materials subjected to low-

velocity impact. Also damage resistance and impact energy absorption are identified as desirable properties if a composite material is to be considered as a viable option for use in structures such as ground and marine vehicles. Recognizing that the cause of low delamination and damage resistance may be due to low inter-laminar integration, this must be demonstrated in conventional composite configurations, while new methods must be proposed and tested to tackle delamination. It must also be ensured that little or none of the conventional materials' advantageous properties are sacrificed in the process.

Conventionally, widely used, unidirectional-fiber based laminated (L) and two-dimensionally woven (2D) composites will be used as a reference to compare properties with newly developed materials. The properties that need to be considered are damage area propagation, impact energy absorption, material stiffness, compressive strength and residual properties after impact. A comparison must also be made between them based on ease of manufacture and effect on final processing to make a decision on the merit of the proposed solution.

The method to tackle delamination in this study is that of three-dimensional woven fabrics. Interlaminar three-dimensional, i.e., quasi-three dimensional, weaves are chosen over through-thickness three-dimensional, i.e., orthogonal three-dimensional, weaves. This is because, in trying to replicate the performance of conventional configurations like unidirectional laminate (L) or two dimensional woven (2D), the former maintains the yarns primarily in the in-plane direction, directly contributing to in-plane properties. Harness number will be

varied in the quasi-three-dimensional specimens to study its effect on performance. This is because higher harness weaves, by virtue of their longer lengths of flat yarns, should possess features closer to the features of the conventional unidirectional configuration. Thin specimens will be used to study the initial properties of the different weaves, due to their relative ease of manufacture. These results will have to be confirmed to be true in thicker specimens too. Explanations for damage modes will be developed based on the experimentation results.

As an end goal for the study, it is hoped that the quasi-three-dimensional weave can be shown to be competitive in performance compared with conventional weaves, while out-performing them as far as delamination resistance is concerned. This will enable fiber-reinforced composites to be exploited for their desirable high stiffness to weight properties, even in applications where previously, they have been ruled out due to the problems of delamination.

1.3 Organization of Thesis

This thesis is ordered into the following chapters. *Chapter 2, Weave Geometries* provides graphical representations of each weave used in this study and explains factors that differentiate one weave from another. *Chapter 3, Sample Fabrication* documents in detail the weaving and curing procedures used to create the samples used in this study. *Chapter 4, Testing Methods* describes the methods used for impact and compression testing, sample inspection and test data processing. *Chapter 5, Presentation of Results* presents the tabulated

and plotted data obtained from impact and compression tests with summary tables and also representative pictures of specimen damage. These results are discussed and analyzed, and their significance explained in *Chapter 6, Discussions.* Finally conclusions from the study are summarized and recommendations for future work in this area are offered in *Chapter 7, Conclusions and Recommendations.* Additional un-presented images of damaged specimens can be found in the *Appendices* section.

CHAPTER 2

Weave Geometries

In this chapter, fiber geometries of the different weave configurations used in this study will be explained in detail. First, a clear definition of the term 'Quasi-three-dimensional' weave is required. This refers to an *angle interlock, inter-laminar* three-dimensional weave. This differs from the more widely seen *through-thickness* three-dimensional weave. Quasi is used to emphasize that these weaves have no through-thickness orthogonal yarns tying all the layers together, but rather, each in-plane yarn serves to hold the layers together, by being integrated into adjacent plies. Figure 2.1 shows this comparison. In the regular three-dimensional weaves, there is some amount of yarn content in the orthogonal direction which does not contribute to in-plane strength of the material. Also these yarns form kinks in the in-plane yarns at points where they are inserted, which, after addition of matrix, form resin rich, damage initiating pockets.

In Quasi-three-dimensional weaves, all the yarns directly contribute to in-plane properties, while still contributing to inter-laminar integration as adjacent layers are woven together to form a three-dimensional network. From Figure 2.1, it can be seen how yarns are interlocked not only with the cross yarns of their own layer, but go deeper into the weave to interlock with the yarn of the neighboring layer.

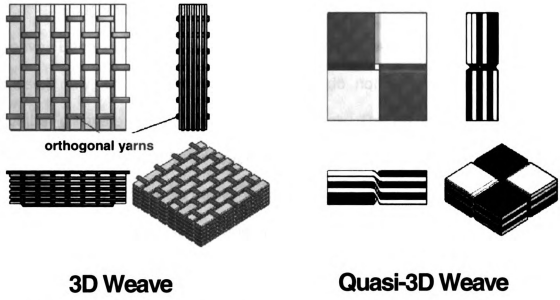

Figure 2.1. Comparison between through-thickness and Quasi-three-dimensional weaves

All samples in this study were of the [0/90] type, meaning that warp and fill yarns were orthogonal to each other. There are two broad categories of samples. In the conventional category, there are unidirectional laminated (**L**) and two-dimensionally woven (**2D**). In the quasi-three-dimensionally woven category, there are two harness (**Q3D**), three harness with offset (**Q3DO3**) and five harness with offset (**Q3DO5**). The inclusions in parenthesis in the previous sentence indicate the nomenclature that will be used henceforth.

Firstly, the difference between ply and layer should be clarified. A ply is a laminar sheet of unidirectional fibers used to build up a laminated (L) specimen. A layer is composed of two in-plane sets of yarns, which are orthogonal to each other (warp and fill) and woven together or with neighboring sets of yarns (i.e., a [0/90] pair). Each in-plane set of yarns that makes up this [0/90] pair will be referred to as a half-layer.

Throughout this chapter, solid model representations are provided of each weave. Each diagram may vary in number of layers. These numbers were chosen only for clarity of description and do not necessarily represent the number of layers used in the tests in this study. The number of layers used in each test will be mentioned when appropriate later on. Each ply/half-layer is represented by a different color for clarity. The diagrams represent the smallest repeating units for each weave from an in-plane point of view.

The sample groups are differentiated from each other by level of integration between layers, offset, harness number and number of layers. These are defined as:

A. *Level of integration*

This describes whether or not adjacent warp and fill yarns, or adjacent layers, are interconnected by yarn content, and to what level. Laminated (L) samples have no integration between adjacent plies, and are held together only by matrix material. Two-dimensionally woven (2D) samples are integrated only within each layer (warp and fill yarns are intertwined), but individual layers are held to each other only by matrix material. These weaves are depicted in Figure 2.2 and Figure 2.3, respectively.

In quasi-three-dimensional samples of all harness numbers, each warp or fill yarn is integrated with the fill or warp yarn above and below it. In this way, each half-layer is held to both neighboring half-layers through positive fiber links, yielding a continuous, integrated network. The maximum depth of any interlock is three half-layers deep (including the ply in question).

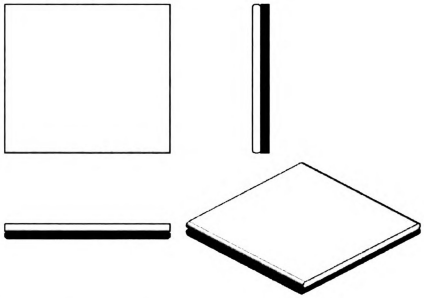

Figure 2.2. L $[0/90]_1$ geometry

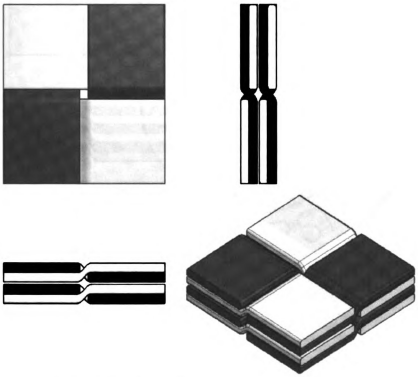

Figure 2.3. 2D $[0/90]_2$ geometry

A two-harness quasi-three-dimensional weave (Q3D) is shown in Figure 2.4. A slight difference might be noticed in the surface yarns which may only be

integrated with the half-layer below (i.e. integrated with only one orthogonal half-layer instead of two). This is an unavoidable consequence which is true of one set of fill and one set of warp surface yarns. The difference in the property of the weave caused by this feature may be negligible in cases with a high number of layers. The level of integration is designated by L, 2D and Q3D at the beginning of the nomenclature.

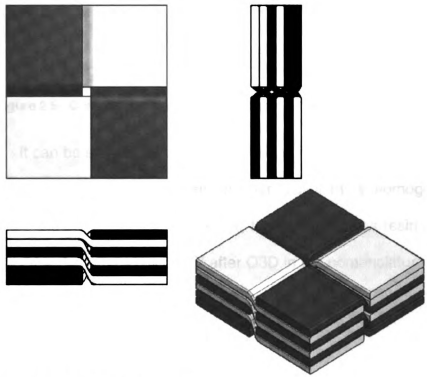

Figure 2.4. Q3D $[0/90]_3$ geometry

B. *Offset*

This describes the shift by one half yarn width, in the position of a tow in relation to a neighboring tow of the same sense (i.e., fill and fill or warp and warp) in the width direction. The difference between an aligned weave and offset weave is illustrated in

Figure 2.5. This is a consequence of having odd harness numbers as the yarns of one layer link with the yarns of the neighboring layer at the midpoint of the unsupported harness. It was done in an attempt to fill up the through-thickness resin rich void between adjacent yarns of one layer by the yarns of the neighboring layers, to yield a more homogeneous through thickness structure.

Figure 2.5. Comparison between aligned and offset weaves

It can be seen from backlit specimens in Figure 2.6, that the weave with offset has no clear regions of resin or fiber, but a more homogeneous composition, while the aligned weave has clear, through-thickness resin areas (lighter areas). Offset is designated by an 'O' after Q3D in the nomenclature.

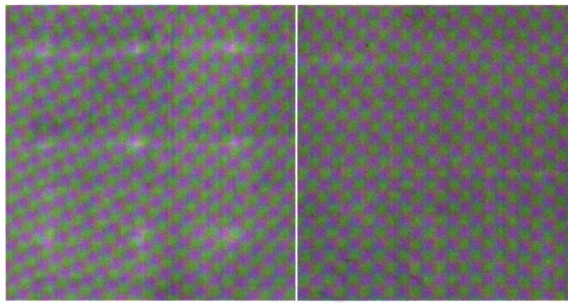

Figure 2.6. Backlit view of aligned and offset weaves

C. *Harness number*

This describes the frequency of interlacing of warp and fill fibers with respect to tow width. In 2D weaves, the fill or warp fibers interlace alternately over and under every orthogonal warp or fill fiber. This yields a two-harness weave as the pattern is repeated every two yarn widths. In higher harness weaves, tows interlace less frequently with the orthogonal tow and have longer regions where they are straight. This can be seen in the three-harness Q3DO3 and five-harness Q3DO5 weaves shown in Figure 2.7 and Figure 2.8, respectively. L samples are considered to have infinite harness number. Harness number higher than two is designated by a number just before the [0/90] in the nomenclature.

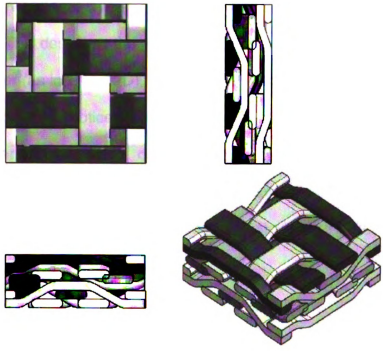

Figure 2.7. Q3DO3 $[0/90]_3$ geometry

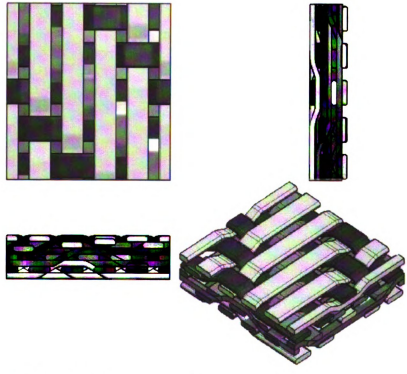

Figure 2.8. Q3DO5 $[0/90]_3$ geometry

D. *Number of layers*

This describes the number of [0/90] pairs that are either stacked one over the other (as in L and 2D), or interwoven (as in all quasi-three-dimensional weaves). It should be noticed that in quasi-three-dimensional weaves, there are in fact, no layers, but a set of orthogonal half-layers. But for clarity of definition, in all weaves, a set of two orthogonal half-layers is counted as one layer. Number of layers is designated by the subscript just after the [0/90] in the nomenclature.

CHAPTER 3

Sample Fabrication

3.1 Prepreg Handling and Weaving

The specimens used in this study were hand woven using hand cut tows or tapes from epoxy pre-impregnated glass fiber sheets or prepreg (CYCOM 1003/W-490). The weaves were made from flat and wide tapes instead of the more conventional eye-shaped cross-section tows. This flat tape with a large aspect ratio (ratio of width to thickness) yields a final product that has less undulation in the fibers allowing each fiber to bear the in-plane loads most efficiently. Also the resin pockets that would be more prominent when eye-shaped tows are used, are greatly reduced. These concepts are depicted in Figure 3.1.

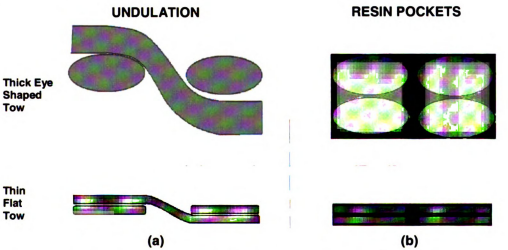

Figure 3.1. Demonstration of lower undulation and resin pockets in flat tape composites

Composite materials with thinner plies or layers tend to have lower tendency to delaminate due to the lower bending stiffness mismatch caused

between layers. This too is an advantage of thin tapes. The disadvantage of thin tapes is that more number of layers need to be woven together to build up the final required thickness.

Apart from the earlier mentioned reasons for using flat wide tapes, prepreg was a very practical choice for hand weaving complex composite specimens as the impregnated resin in it protected the glass fibers and allowed the tows to be handled easily with no damage to them as long as they were treated with some amount of care. If weaving was attempted just using regular tows of unprotected glass fiber or glass roving with just a sizing layer, they would be more prone to damage due to the manipulation and abrasion, and the final product would have lower quality.

The prepreg used in this study comes in the form of a roll of continuous flat glass fiber sheet (with fibers all aligned along the direction of tape) with uncured epoxy impregnated into it. The roll was about 150m (144 yards) long and about 0.3m (12") in width, with the tape thickness of 0.25mm (0.01"). The tape is backed by a waxed paper sheet which keeps the layers of the roll separate and helps with handling and cutting until the layup is done. It was kept in an airtight bag with silica gel to keep moisture away when not in use. The bag was stored in a freezer at 0°C until the prepreg was required. This is a recommended storage procedure to prevent the epoxy in the prepreg from becoming sticky and curing prematurely. When the material was required, it was removed from the freezer, without opening the bag, and allowed to defrost to room temperature, which took up to an hour. The reason for keeping the bag

sealed until the material was at room temperature was to make sure that condensate was not allowed to form on the prepreg causing water damage.

Once at room temperature, the prepreg with the backing sheet still on, was gradually unrolled on a cutting mat, and pieces were cut off based on the size of sample to be made. In this study, it was decided that in order to have the highest control over the yarn placement and orientation in the samples, each 125mmX125mm (5"X5") sample would be prepared individually, as opposed to other similar studies where larger plates were prepared from which samples were cut. This also made the weaving less cumbersome and required less harmful manipulation of the yarns. Figure 3.2 shows an example of a Q3DO3 sample just after weaving. It can be seen that there is a high degree of alignment and regularity of the yarns, along with very tight fiber packing with negligible gaps between adjacent tows (approximately 0.5 mm in this sample).

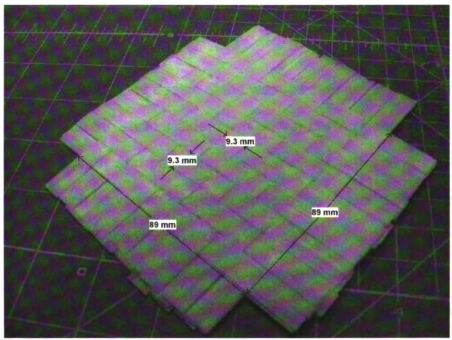

Figure 3.2. Example of hand woven 3DO3 specimen before curing

The prepreg was cut using a rotary cutter for clean cuts. A dimensioned cutting mat like the one seen in Figure 3.2 proved to be very convenient when cutting pieces of specific dimensions. It is very important that the room in which the prepreg is being handled is cool (13°C or 55°F). If the temperature is warmer, the prepreg tends to become sticky and soft and it is difficult to handle. At a temperature around 13°C, the surface of the prepreg is dry and non-sticky, and the strips which will be cut have a convenient stiffness to them, which helps in manipulation during weaving. It was considered good practice to cut many pieces of the prepreg at a time from the parent roll and store them in separate airtight bags containing enough pieces for one session of weaving. This prevented the main roll from having to be defrosted every time a piece was needed which would cause a degradation of properties due to thermal cycling. This way, even the individual bags were stored in the freezer till required. The smaller bags of material also took less time to defrost and thus could be removed just before they were required.

Based on the design of the weave being made, the pieces of prepreg were placed with the stickier side down on the cutting board (once the backing sheet was removed) and cut along the fiber dimension into strips of 9.3mm (0.375") width which served as individual yarns in the weave. This dimension was decided upon so that there would be eight unit cells within the 75mmX75mm (3"X3") section of the sample exposed in the impact testing holder. It helps if the square being used as a guide for the cutter is slightly above the prepreg and not touching it, otherwise it tends to stick to and damage the material. The strips

were then used to weave together the samples following procedures explained later. The final product from weaving was similar to that seen in Figure 3.2.

In this study, three types of weaving procedures were used based on the type of weave. In the case of the 2D weave, each layer were produced individually and then placed over the other with good alignment (referred to as type 1). For the higher harness quasi-three-dimensional weaves (Q3DO3, Q3DO5), the specimen was built up one half-layer at a time, with the new half-layers being formed and integrated into the lower orthogonal ones, and thus into the entire sample (referred to as type 2). In the case of the two-harness Q3D weave, this method was not feasible as the lengths of free, unwoven yarns in the upper most half-layer were not long enough to be raised as required to insert the cross yarn, without damaging the fibers or distorting the weave. In this case, the specimen was built from centre of the specimen outwards with all layers through the thickness at that cross section being produced simultaneously (referred to as type 3). It is understood that there is no explanation required for L samples where each ply is just laid over the last at right angles to it.

The simplest type of weaving method which was used for 2D specimens is type 1, depicted in Figure 3.3.

1. First, the yarns of the warp direction were laid down on an adhesive strip to hold them in position.

2. It proved to be easier to carry out the next steps if the tapes were placed with their stickier sides facing up. Using a long, thin tool, the alternate yarns were split. The tool was used to gently push back to create adequate place for the fill

yarn to fit. Due to the stiffness of the yarns, they held their position long enough to carry out the next steps. The fill yarn was inserted into the gap, and brought as close to its final position as possible.

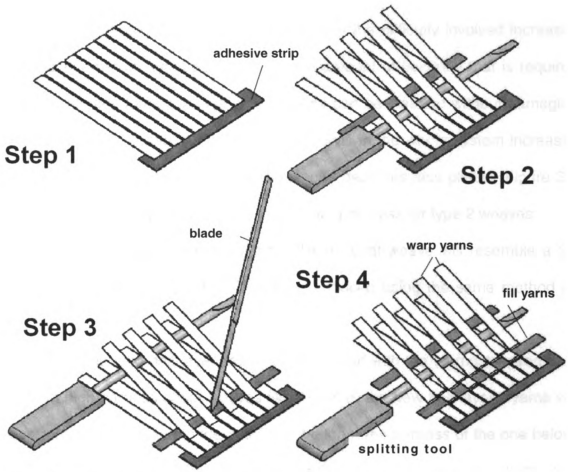

Figure 3.3. Weaving procedures for type 1 weave

3. Now the tool was slid up to support the gap wide enough so that a blade edge could help with 'packing' the yarn as tightly into the wedge. If this is done with care, no damage is caused to the tape.

4. Alternate yarns was raised and the procedures repeated. This method can be used for 2D weaves of any harness number.

For weaves of type 2 (all higher harness quasi-three-dimensional weaves) a half-layer-wise approach was adopted as every new ply was integrated into the previous topmost layer. Figure 3.4 describes the steps involved in the first two layers of a Q3DO5 weave. The process can be just repeated for as many layers as needed. It should be mentioned though, that the difficulty involved increases with the number of layers as there is some amount of flexibility that is required from the already formed weave so that yarns can be inserted without damaging or deforming the weave. As the number of yarns in the whole system increases and owing to their slight stickiness, the weave becomes less pliable. Figure 3.4 depicts a step-by-step procedure of the weaving process for type 2 weaves.

1. The first layer of any quasi-three-dimensional weave will resemble a 2D weave of that harness number. This was produced using the same method as with type 1

2. Now the next half-layer had to be integrated with the topmost woven half-layer. In high harness offset weaves like this one, the new half-layer's yarns will be introduced below and in the middle of the long free harness of the one below. The yarn was introduced by carefully lifting the lower yarn span up with the tool and sliding the new yarn in while simultaneously sliding the tool out.

In the figure it might appear that the yarn is being unduly stretched, but in reality, as mentioned before, the whole weave deflects a bit. The yarn being lifted will slide a bit out but once the step is complete, it can be nudged back into its original position.

3. This was repeated till the entire half-layer is constructed.

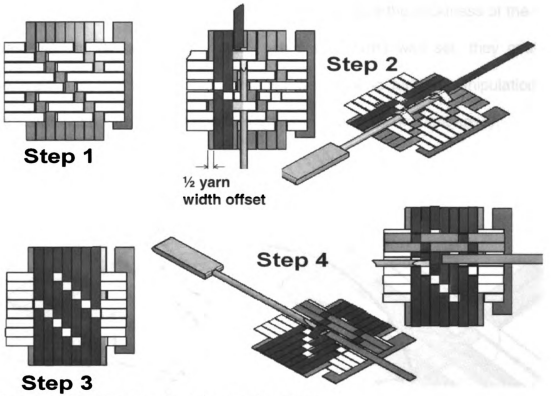

Figure 3.4. Weaving procedures for type 2 weaves

4. Once this half-layer is ready, the next set of yarns is introduced similarly at 90˚ to the last set. During the entire process, the adhesive strip to which the first layer is attached helps hold the assembly in place.

The samples of type 3 require the most amount of dexterity to weave as weaving of the complete thickness is done simultaneously at each cross section. First, each yarn needed to be 'capped' with adhesive tape. This was to prevent the yarns from sticking together and facilitate easy splitting of the yarns when inserting the cross yarns. This also made it easier to differentiate between layers as all six were dealt with simultaneously. The procedure is depicted in Figure 3.5.

1. The weaving was begun from the center of the sample. The center four yarns (all 6 layers) were placed as shown. In this case the stickiness of the yarns was used to an advantage. After each set of yarns was set, they could be pressed a bit which held them together well making further manipulation less delicate as the yarns would not dislodge from their positions that easily.

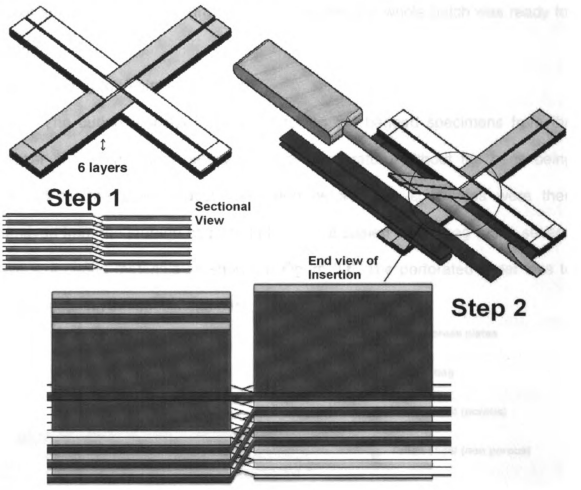

Figure 3.5. Weaving procedures for type 3 weaves

2. Now the weave was formed step by step going outwards in all directions. A tool was used to split and hold apart the yarns while the cross yarns were inserted, starting from the bottom yarn in a set and moving upwards. The magnified end view in Figure 3.5 shows the cross section of the area being

woven at that point and the way in which the yarns need to be separated in order to get a quasi-three-dimensional weave. Once the entire sample was formed, the edges of the yarns with the adhesive tape were cut off so that the tape did not go into the curing process.

Once each specimen was prepared, it was placed within a waxed paper sheet and stored in an airtight bag in the freezer till a whole batch was ready for curing.

3.2 Curing for Thin Specimens

The curing process involved removing the bagged specimens from the freezer and letting them defrost to room temperature without the bags being opened for the same reason as stated before. The specimens were then removed from the storage bags and placed in a sealed curing bag within several layers of curing materials as shown in Figure 3.6. The perforated mylar was to make releasing the specimens easy, while still allowing

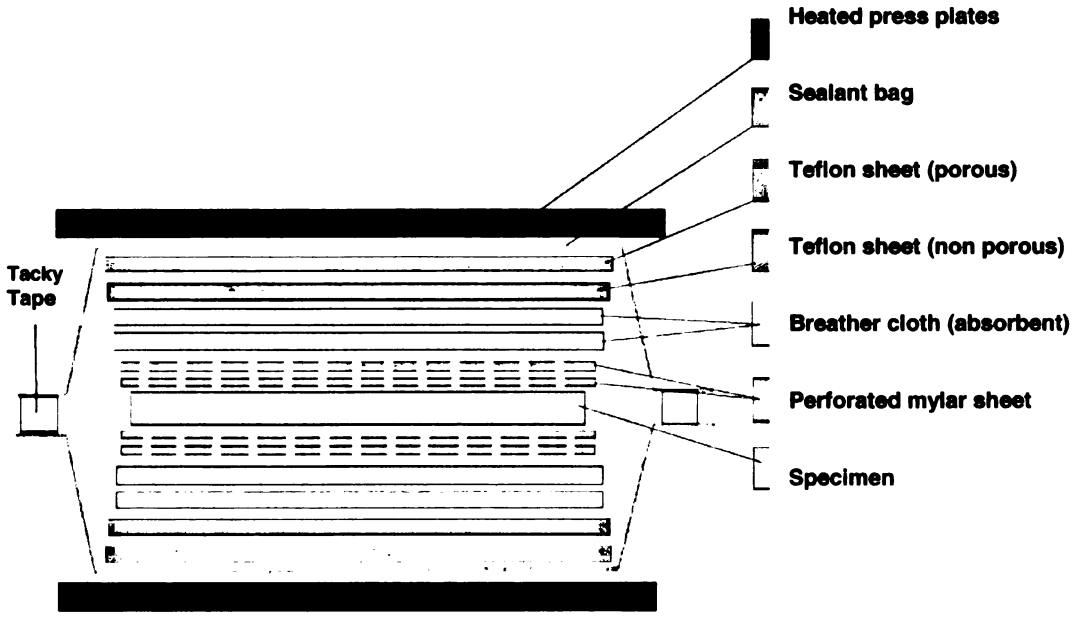

Figure 3.6. Curing bagging procedure for thin specimens

excess resin to flow to and get absorbed by the breather sheets. Extra layers of Teflon coated fabric were introduced on either side to prevent any adhesion of the specimens or liquid resin to the sealant bag.

This whole layup was placed in a *Tetrahedron* hot press and a pressure of 0.55MPa (80psi) was applied to the specimens. The temperature was ramped up from room temperature to 160˚C (320˚F) at 5˚C/minute. It was held at this soaking temperature for 45 minutes before being ramped back down to room temperature at the same rate. The specimens were removed from the bag, mounting holes were drilled and they were now ready for testing.

3.3 Curing for Uniform Thickness

Apart from the 2mm samples that were prepared as described above, later in the study, the need arose for samples that were thicker (~6mm) and with a lower fiber volume fraction (~50% as opposed to the previous ~70%). These samples (whose nomenclature begins with Th which is short for Thick) were woven in the same way as the previous samples, but the curing process was modified so that each batch had a repeatable fiber volume fraction, flatness and thickness.

In the previous method, as a large force was applied directly to the specimens during curing, when the resin liquefied, it squeezed out of the prepreg causing higher fiber volume fraction. Using this method there was no control over the thickness (although thickness was within acceptable limits of deviation for the tests). The thick samples were cured in a specially built curing die, which had

thickness control dams which separated the upper and lower press plates as shown in Figure 3.7. The dam was the dimension of a finished sample.

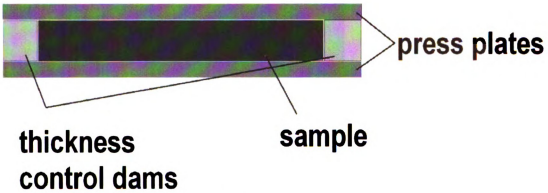

Figure 3.7. Curing die for thick specimens

The woven prepreg sample was trimmed neatly to the square dimensions of the pocket in the die. Knowing the thickness of each cured ply (0.25mm), the dam was dimensioned to have a height equal to the sum of the plies so that there would be no resin loss due to squeezing of the plates together. The plates would be pressed together in the hot press to compact the uncured sample into its final shape, after which, the dams restricted any further compression, while maintaining the shape of the specimen. This way, the samples that were produced had approximately the same fiber volume fraction as is specified by the manufacturer (~45%), identical shape and thickness and flatter, more uniform surfaces. Peel ply was used to line the die so that extraction of the sample was made easy. As these samples were thicker than the last, the soaking time in the curing cycle was increased from 45 minutes to 100 minutes, to make sure that the specimen was cured even on the inside.

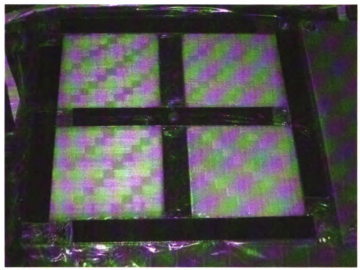

Figure 3.8. Thick specimens in curing die

An edge replication method was used to visualize the through-thickness composition of cured samples of each weave to gauge the quality and uniformity of the final products. The method began with cutting an edge of the specimen, sanding it flat with 1200 grit sandpaper (with water to prevent burning the surface), and then polishing it on a polishing felt cloth (placed on a flat glass) with 5 micron and then 3 micron polishing powder mixed with a little water. This yielded a smooth shiny cross-section surface. Now using a syringe, acetone was injected onto the smooth edge. Immediately a piece of edge replication tape was placed on the surface (without any sliding), and pressed against it with a soft rubber block till the acetone evaporated fully. Now the texture of the cross-section of interest would be imprinted on the tape, which could be magnified, viewed and printed off from a microfiche reader. Figure 3.9 (on the following page) shows the edge replications of the five sample groups. The width of samples presented is the maximum that the microfiche reader is capable of

displaying. The thicknesses in all cases are 2mm but the diagrams have been stretched to make the structure clearer.

***NOTE**: Any nomenclature seen on the samples in the figures is to be ignored as samples have been re-arranged and re-named for the purpose of this thesis.*

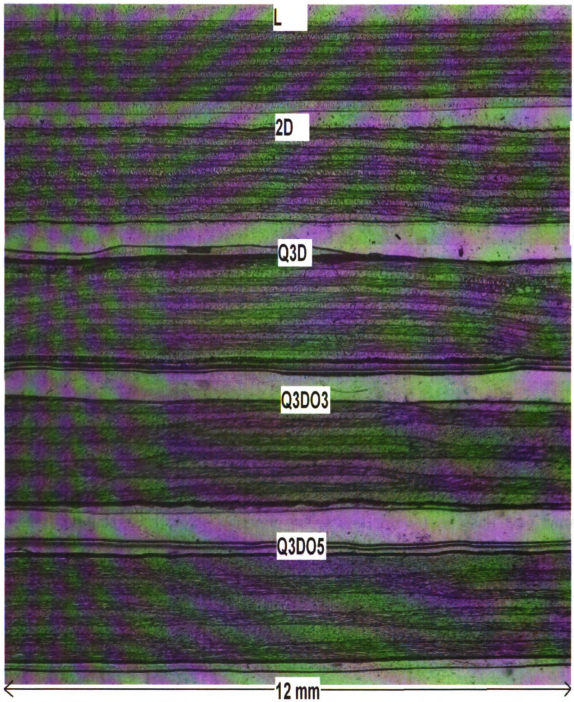

Figure 3.9. Edge replication of the different weaves

CHAPTER 4

Testing Methods

In order to characterize the impact and post-impact performance of each weave type, a series of tests were run on small, thin coupons of each type. The tests included impact characterization using a drop weight tester, damage assessment by back lighting, determination of fiber volume fraction by Archimedes' principle and characterization of in-plane compressive properties pre and post-impact using a compression test. Later in the study, to verify the processes presented, impact tests were run on thicker samples of the different weaves. Each of these methods will be dealt with in detail in this chapter.

4.1 Impact Characterization

4.1.1 Drop Weight Tester

In order to measure the impact energy absorption capability and the impact characteristics of the different weaves, specimens of each type were subjected to impact tests. The impact tests were carried out on a standard *DYNATUP 8250* instrumented drop weight tester, with the attached data processor using the *920* version of software. Figure 4.1 shows a schematic of the set up along with all key elements.

The basic setup consists of an instrumented drop weight with a tup attached to its end. The weight is guided on a pair of polished slider rods to ensure accurate, controlled and low friction fall. The force sensed by the tup is measured by the force transducer.

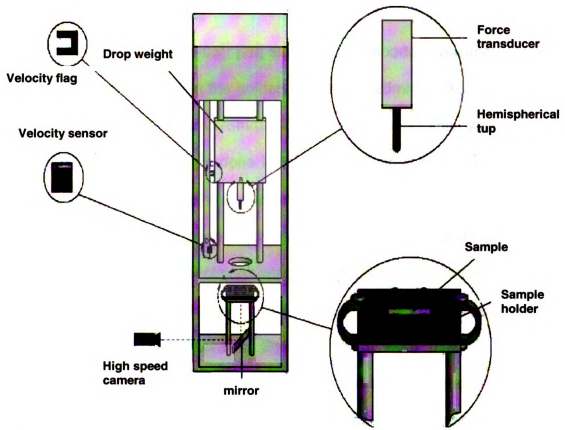

Figure 4.1. Drop Weight Tester Schematic

ASTM standard D 7136/D7136M- 05$^{\varepsilon 1}$ [28] recommends an impactor tup diameter of 16mm. Recognizing that the response of a composite specimen to impact would vary based on the tup diameter [25], the tup used in this test was of the same diameter as the yarn width used to weave the specimens, which was ~9mm (3/8"). This was chosen so that direct relation between tup diameter and yarn width was established, enabling results to be scaled to other tup sizes or yarn widths in further tests. Later in the study, the tup diameter was increased to 12.5mm (0.5") when impacting the thicker specimens with the same cell size. This was done in order to induce a larger delamination area, in the hope that this would better differentiate the behavior of the different samples tested.

4.1.2 Specimen Dimensions

ASTM D7136/D7136M-05$^{\varepsilon 1}$ [28] standard unsupported specimen aperture (area of specimen exposed in the holder) is 75mmX125mm (3"X5") [28]. In this study, an aperture of 75mmX75mm (3"X3") was used. This was to have consistency with previous tests done in this area for direct comparison. It was also felt that the unequal lengths of specimen in the two in-plane directions would lead to unequal stiffness in each direction, resulting in unequal damage fields. It seemed more apt to study specimens which had equally supported lengths along their fiber axes. Due to ease of manufacture of more complex quasi-three-dimensional weaves, specimens of 2mm thickness were used in the initial studies, and specimens of 6mm thickness were used in the second portion of the study. This is different from the 5mm thickness that is suggested in the same ASTM standard.

As a concluding test for this study, to verify concepts learned from thin samples, 6mm thick, dimensionally accurate samples of L, 2D, Q3DO5 and a modified five-harness Quasi-three-dimensional weave were also impact tested in a similar manner to the thin samples.

4.1.3 Specimen Holder

The expanded view in Figure 4.1 shows the clamping method for the specimens. ASTM D7136/D7136M-05$^{\varepsilon 1}$ [28] standard fixture for holding the specimen is based on 4 rubberized toggle clamps holding down the specimen. However this method may not provide sufficient pressure to prevent the sample from slipping. Lee *et al* [29] found that due to this, absorbed energy was a

function of clamping pressure, with some of the absorbed energy readings with slippage being 4.5 times that without slippage. Also in this study, the specimen thickness is thinner than that ASTM specified 5 mm (here specimens of 2mm thickness were used). This gives the specimens more of a tendency to 'flow' and thus more easily slip from the clamps. To prevent any such slippage in order to have consistent readings, all specimens were drilled and bolted between two rigid plates at eight points as shown in Figure 4.1. These bolts, apart from positively locking the motion of the specimens also clamped the plates tightly together thus spreading the boundary loading of the specimen to more points along its outer edges. This whole rigid setup was then held to the impact tester by toggle clamps.

4.1.4 Data Acquisition and Processing

The data recording is triggered by a velocity flag and sensor system, which is also used to calculate initial tup velocity (v_i) at impact. These are shown in Figure 4.1. The flag has two blades at a known center distance of 10mm from each other designated as s. These blades interrupt the photo diode based sensor which shows up as a velocity step for the period of blockage of the sensor. It is positioned such that at the moment the falling tup contacts the specimen, the leading edge of the second blade has triggered the sensor. This ensures that the contact-impact velocity is calculated accurately before the effect of deceleration due to contact with the specimen is felt. Using the time period between the onset of voltage spikes from each blade (t_b), this initial impact velocity (v_i) is calculated by using the simple formula:

$$v_i = \frac{s}{t_b} \tag{1}$$

Once the first blade of the flag passes over the sensor, the time and force data starts to be recorded. The force transducer records voltage levels which are later multiplied by a calibration factor and divided by any amplification gain used, to yield force values. Using these force values, F(t), and mass of the drop weight, acceleration at every time instant, a(t), can be calculated as:

$$a(t) = \frac{F(t)}{m} \tag{2}$$

The output from the tester's software contains several thousand data points consisting of time, force and displacement data. This displacement which is automatically presented by the machine, is calculated by first calculating velocity at time t using the relation:

$$v(t) = v_i + \sum_0^t a\,\Delta t \tag{3}$$

Here Δt is the time between samplings. Using this, the deflection history, $\delta(t)$, can be calculated by summing the velocity history using:

$$\delta(t) = \sum_0^t v\,\Delta t \tag{4}$$

4.1.5 High-Speed Photography

In this study, in addition to recording time and force histories, a high-speed camera was also set up to capture the damage process visually aiming at extracting useful information from it. From lack of space, and in order to prevent damage to the camera from flying debris due to impact of the specimen, the camera was placed at a distance from DYNATUP setup, and the underside of the

specimen was viewed by using a mirror at 45° to the vertical as seen in Figure 4.1. Powerful lights were shone onto the bottom surface of the specimen to capture the event clearly. The camera was run at 4000 frames per second which yielded one frame every 0.25 msec of the damage event. It had the capacity to record a maximum of four seconds duration event. Frames from this recording were easily matched with different points in the load-deflection curve outputted from the impact tester. This was done by first choosing the frame which corresponded to initial contact of tup with the specimen. As the specimens are thin, this is clearly seen as a deflection in the under side of the specimen. Once this reference zero-frame (frame right before the initial-contact frame) was identified, each frame could be extracted and tied to the corresponding point on the load curve. The recording time for each frame is stored, so calculating time of frame with respect to the zero-frame is simple.

4.1.6 Impact Energy

Impact energy absorption and resistance to damage propagation of different weaves in low-velocity perforation was of most interest, so impact energies higher than the expected energy absorption were supplied to ensure that perforation occurred. Some authors [1, 25] have shown that impact response is dependent on incident impact energies. So in order to have a fair comparison between samples, all tests on the thin samples were run by dropping the weight from a height of 500 mm with the same carriage mass of 12.86 kg. This caused the impactor to have an initial striking velocity of 3.1 m/s and an impact energy of 61.79J. For the thick specimens, initial tests with the maximum allowable weight

of 15.9 kg and height of 1m showed that this was insufficient to perforate. In these tests, additional velocity was provided by a pneumatic pressure attached to the drop weight to increase its velocity to 7.5 m/s.

4.1.7 Summary of Impact Testing

To summarize the general testing procedure, each sample was bolted between the mounting plates, and the assembly was then clamped onto the machine. The drop weight was carefully lowered and the tip of the tup was used to position the sample before clamping to ensure that impact was centered. It was also verified that the velocity flag was at the required position such that the leading edge of the second flag was just triggering the velocity sensor when the tup was touching the specimen's surface. Now the drop weight was raised and locked into position. When ready, both the drop weight and the camera were triggered manually at approximately the same time. The impact event takes under 200 msec to complete and the camera has approximately four seconds of recording time. Thus, the triggering of the camera is not critical as long as it is started along with or before the impactor is released. The first blade of the flag on the drop weight triggered the velocity sensor as well as the data acquisition system at the right moment, to start force and time recording, while damage behavior was recorded by the camera.

4.2 Testing Results

4.2.1 Load Deflection Curve

The desired output was a load-deflection curve as shown in Figure 4.2. It can be seen that there is an ascending and a descending portion to it. The load

and time histories of the tests may contain oscillations due to two main sources. The first is higher frequency 'ringing' of the impactor at its natural frequency, which does not typically represent an actual force transmitted to the specimen. However, the lower frequency flexural vibrations of the impacted specimen like the ones seen in Figure 4.2 are actual forces applied to the specimen and should not be filtered or smoothed [28].

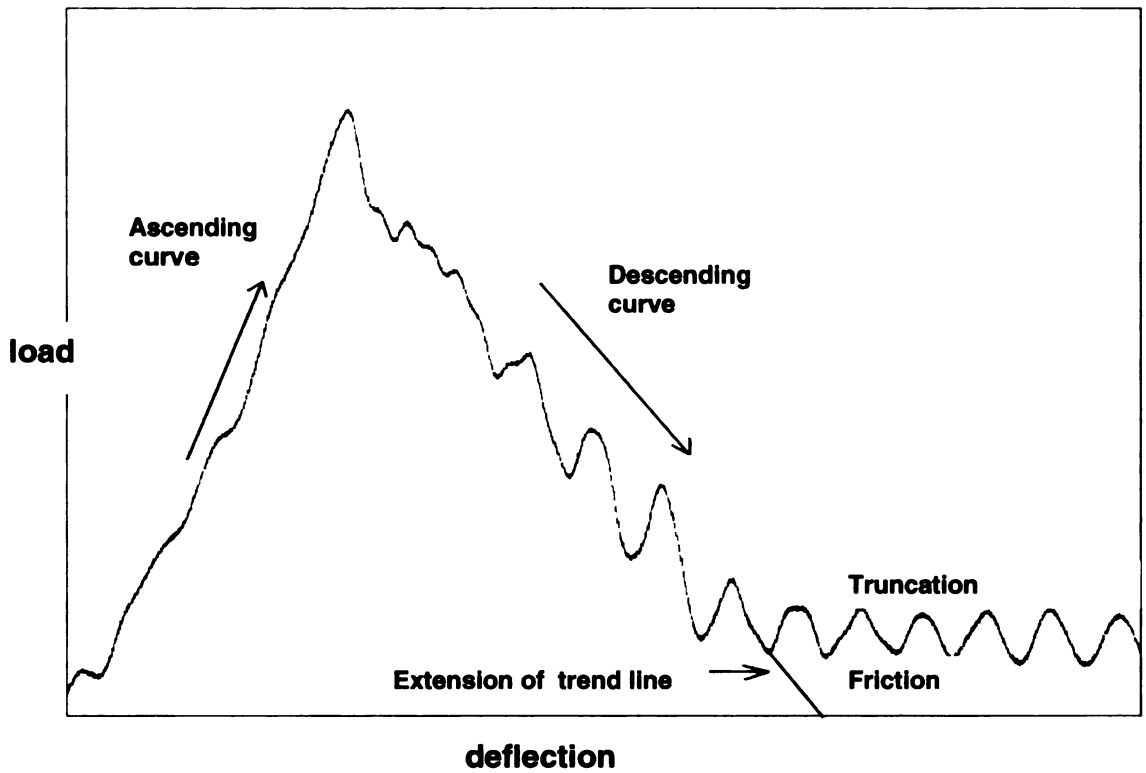

Figure 4.2. Typical load-deflection curve showing truncation

It can be seen that after the descending portion of the plot, the force does not drop to zero as would be expected. This is because once the tip of the tup has perforated the specimen, there is friction between the hole in the specimen and the sides of the long tup. This part of the curve does not represent energy absorption due to the damage process of impact and must be removed. To do

so, a trend line is developed from the data points toward the end of the descending portion of the plot, and extended to the zero force line. This is an accurate representation of only damage induced forces and deflection that might be produced from just a spherical impactor. Figure 4.2 shows this truncation. All data points after the extension line are dropped from further analysis.

4.2.2 Impact Characteristics

There are several useful quantities that can be measured from the final truncated load-deflection plot. Peak load is the maximum load felt by the impacting tup. The ascending half of the curve consists of two separate segments as shown in Figure 4.3. The slopes of these two segments are designated at 'slope 1' and 'slope 2'. Maximum deflection is the deflection at the point where the trend line extension reaches the zero load line. The area under the curve represents absorbed impact energy, calculated by integrating the force values within the zero-max deflection range. This is seen as the shaded area in Figure 4.3.

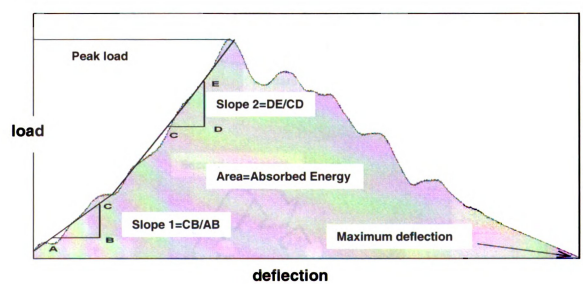

Figure 4.3. Measured quantities from load-deflection curves

4.2.3 Determination of Damage Area

As the specimens used in this study were thin and translucent, internal damage could be identified using back lighting method. There were two types of damage areas that were measured. Primary damage area, which corresponds to through-thickness damage in the specimen, was identified by the dark region seen in the backlit photographs of the specimen. The area was approximated by simple geometric shapes, whose dimensions were determined using known mounting hole pitch as reference. An example of this *primary damage* area is shown in Figure 4.4 as the circled area. From Figure 4.4 , it is also possible to see a lighter outline of horizontal extended damage. This is the *secondary damage* area, which corresponds to the delamination-like fiber stripping damage caused in the rearmost ply or plies. Depending on the weave integration, this damage may spread to more than just the last one ply.

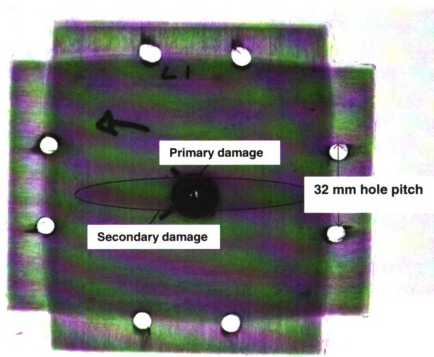

Figure 4.4. Primary Damage Area

In many previous studies, a projected area approach was taken to measuring damage area, where the damage areas from all layers were projected onto one plane and that area measured. It was felt that to be more accurate, the damage areas should be split into through-thickness damage area and rear damage area. This is because the much smaller *primary damage* area affects all the layers through the composite's thickness, while the *secondary damage* area only affects one or a few layers. The secondary damage area was measured by approximating the damage on the rear surface of the sample by a combination of geometric shapes. This is shown in Figure 4.5.

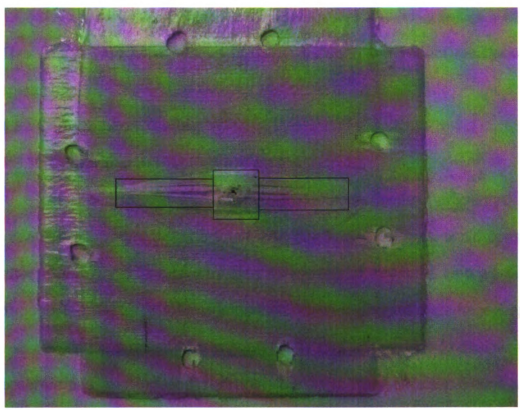

Figure 4.5. Secondary damage area

4.2.4 Specific Energy Absorption

In order to have a comparison between the different weaves of the energy absorption capabilities taking into account the damage area, a quantity called specific energy absorption (SEA) was introduced. This is the energy absorption with damage area as the normalizing factor. Now since *primary damage* area affects all the 6 layers through the thickness, while *secondary damage* area only affects the rear most layer (which includes primary area for the last layer), it was decided that a fair quantity to normalize the energy absorption of each specimen by, was a weighted combination of the two damage area measurements. Thus SEA was calculated in each case as:

SEA = Absorbed Energy / [(11 X primary damage area)+secondary damage area] (5)

This only serves as a relative measure between the impact resistance of the specimens.

4.3 Compression Testing

4.3.1 Compression Fixture Version 1

In order to characterize the post-impact residual properties of each impacted specimen, the specimen was put through a quasi-static compression after impact (CAI) test. Undamaged specimens of the same type were also put through the same test for comparison. Each damaged/undamaged specimen was installed in a multi-piece support fixture that was aligned to minimize loading eccentricities and induced specimen bending. The specimen-fixture assembly was placed between flat platens and end loaded under compression until failure.

The test is designed to uniaxially load the specimen in the plane while load-deflection data is recorded.

The first support fixture was built according to the concept of the ASTM D7137 test, although its dimensions were very different, to accommodate the much smaller specimens used in this study. This is depicted in Figure 4.6. It is recommended that the damage size be limited to half the unsupported specimen width (width of specimen in the gap between upper and lower halves of the fixture) to minimize interaction between damage and edge related stress/strain fields [30]. In these tests, the width of specimen was 75 mm which was 3 times the largest diameter of primary damage (through thickness damage) although the secondary damage may have been larger and in a few cases, as wide as the specimen itself. The specimen dimensions were 75mm X 75mm (3"X3"). This was different from the 100mm X 150mm (4"X6") specimen size suggested by the ASTM standard. Also, specimens had a thickness of 2mm instead of 5mm. Figure 4.6 shows a model of the first test fixture that was built.

It consisted of an upper and lower section. The sample was held in place by support plates on all four sides. All bolted components were adjustable within a small range to accommodate varying sizes of specimens. The two side support plates contacted the specimen only through knife edges. This was designed so that the fixture prevented the specimen from global buckling under the load, but was lightly clamped enough to prevent the specimen from being unduly constrained. Thus the specimen could slide and deform under the load in-the-plane.

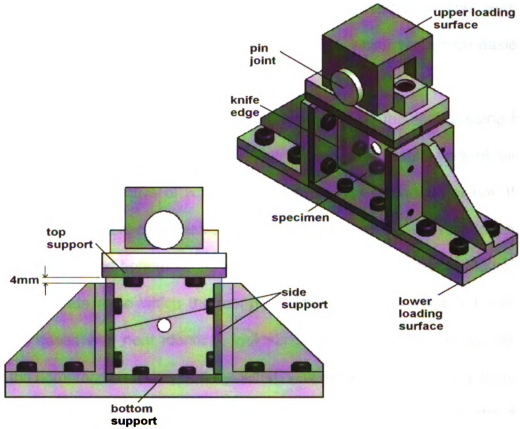

Figure 4.6. Compression fixture version 1

There was a gap of 4mm between the top and side supports to allow for the compression deflection during loading. Once the specimen was clamped in this fixture, the whole assembly was placed between the platens of a compression testing machine, and quasi statically loaded until failure. There was one big difference that was introduced into this test fixture that was not noticed in any other study. This was the pin joint on the upper compression plate. The reason for this is that in a fixture without a pin joint, the loading edges of the sample need to be parallel to a high degree of accuracy. If not, there will be uneven loading across the width of the sample which will yield erroneous results due to stress concentrations. The introduced pin joint would take up any

unnoticed lack of parallelism between the loading surfaces. This was all considering that the edge of the specimen was flat, which was much easier to achieve by polishing the edge on a flat buffer.

Some preliminary compression tests were run on this fixture using both damaged and undamaged samples and some unexpected results were obtained. In every case, irrespective of whether the sample was perforated or not, there was failure due to local compression buckling at the loading site in the free span between the top and bottom sections of the fixture. This is shown in Figure 4.7. Also the ultimate force which the sample sustained in both impacted and un-impacted cases was near identical, indicating that the impact damage did not affect the compression damage. If the fixture was suitable for this application, the damage would no doubt have occurred at the weakest section of the specimen which is the perforated zone.

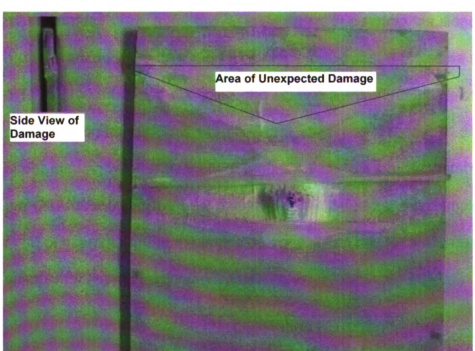

Figure 4.7. Unexpected damage pattern after using compression fixture 1

On further investigation, it was noticed that other authors too had faced similar problems. The problem lies not with the fixture per say, but with its usage with thin specimens. Liu *et al* [22] ran into the same problem when testing thin specimens in a similar NASA fixture which had two free regions at the top and at the bottom of the specimen. Sanchez-Saez *et al* [4] conducted studies on several CAI test support fixtures and found that using the ASTM fixture tended to cause failure of the specimen near the top support instead of the central impact damaged area. They suggested using a fixture which had the unsupported region in the center, forcing the damage to occur at the region of damage.

4.3.2 Final Fixture

A second test fixture was built along the lines of the suggestions of Sanchez-Saez *et al*, with the addition of the previously mentioned pin joint for the same reason. Figure 4.8 illustrates the new test fixture.

In this fixture, there are no knife edges supporting the sides of the sample, but they are supported by the faces of the side support plates as shown in Figure 4.8. To prevent undue clamping, the screws holding the side plates in place are only hand tightened. This will allow the specimen freedom to slide and deform under loading without restriction. Figure 4.9 shows a representative sample from the CAI tests using the new fixture. As can be seen, the samples failed at the point of interest around the impacted zone. Thus this form of fixture is considered suitable for testing thin composite samples.

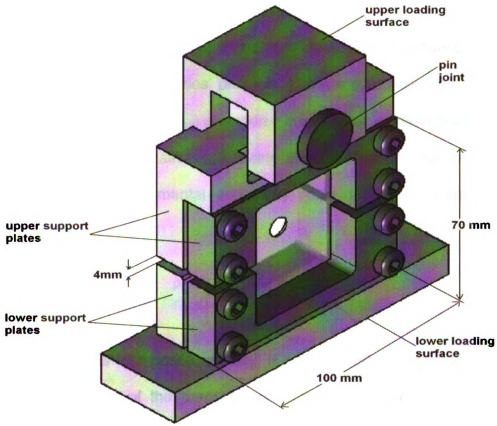

Figure 4.8. Compression fixture version 2

Figure 4.9. Sample tested with compression fixture 2 showing damage along center line

4.4 Determination of Fiber Volume Fraction

Fiber volume fraction (v_f) was determined by first measuring the density of the material using Archimedes' principle. Using a standard setup, the weight of the sample is measured (w_{dry}) and then it is immersed in clean distilled water and its weight measured again (w_{wet}). Using these values and the exact density of water at those experimental conditions (ρ_w), density of composite (ρ_c) is calculated as:

$$\rho_c = \frac{w_{dry}}{\left(\frac{w_{dry} - w_{wet}}{\rho_w}\right)} \tag{6}$$

Once this composite density is determined, using the manufacturer supplied densities of the prepreg's constituent fiber and resin (ρ_f=2.54 X10^3 kg/m^3 and ρ_r=1.21 X10^3 kg/m^3 respectively), fiber volume fraction of the composite is determined as:

$$v_f = \frac{(\rho_c - \rho_m)}{(\rho_f - \rho_m)} \tag{7}$$

CHAPTER 5

Presentation of Results

In this chapter the results and composite plots for each specimen type and test will be presented. Representative photographs will be presented for each group, while the entire collection of photographs (which might prove cumbersome to include in this chapter) are contained in the appendices.

5.1 Impact Tests

5.1.1 Load-Deflection Curves for Thin Specimens

Following are the load-deflection curve groups for the five groups of thin specimens subjected to drop weight impact tests. These are presented to show the distribution or variation within each set, and the general trends in each case. Trend lines that are superimposed on the plot sets highlight these trends.

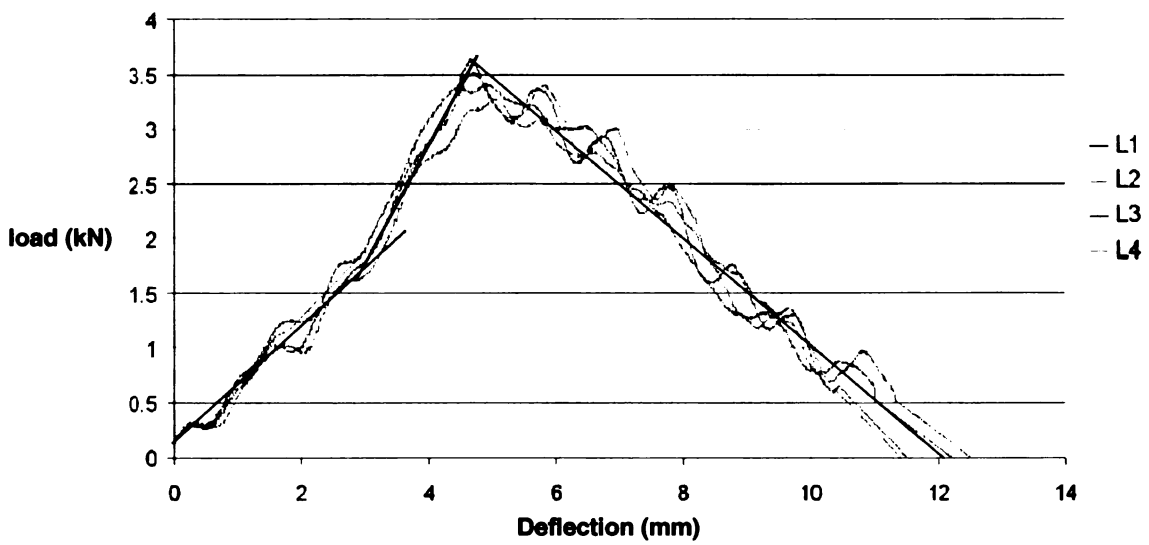

Figure 5.1. Load-deflection curves for L specimen impact tests

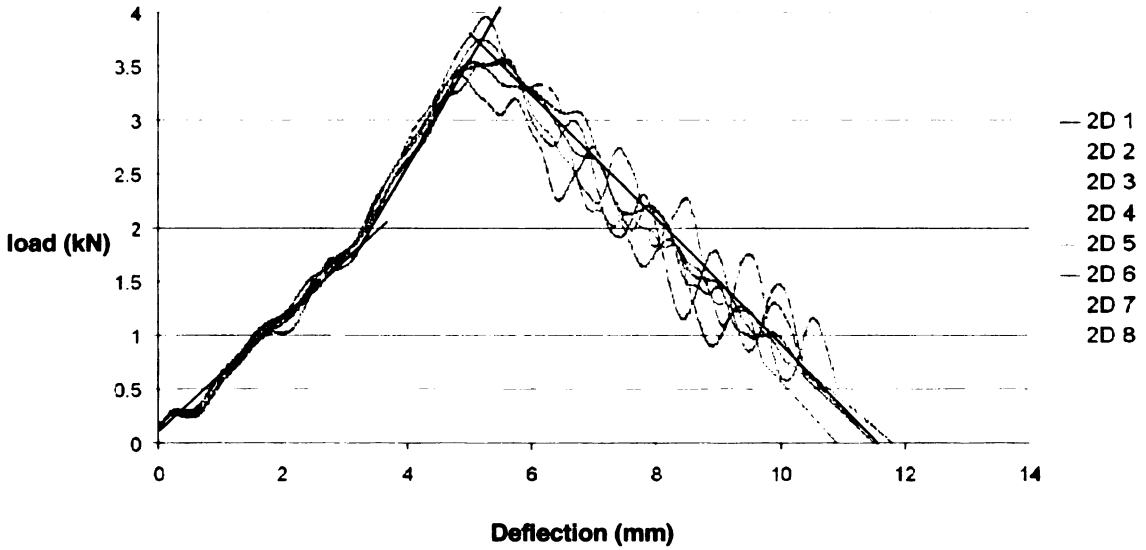

Figure 5.2. Load-deflection curves for 2D specimen impact tests

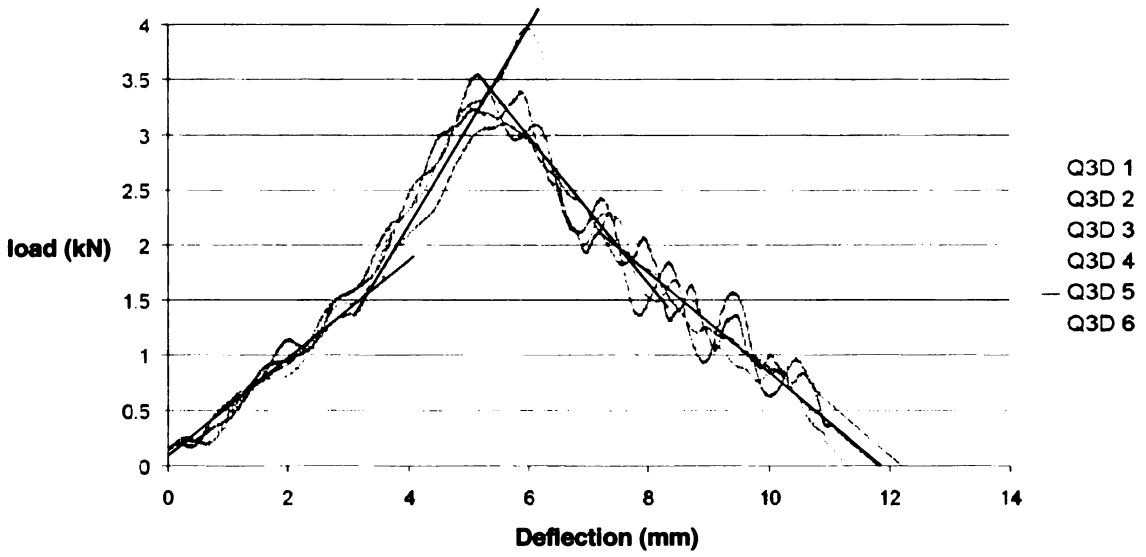

Figure 5.3. Load-deflection curves for Q3D specimen impact tests

From the plots of L, 2D and Q3D weaves shown in Figure 5.1, Figure 5.2 and Figure 5.3, respectively, it is seen that the load values increase along the ascending portion until peak load is reached. At this point, the load begins to drop at a significant rate immediately. In the case of the Q3DO3 and Q3DO5 samples shown in Figure 5.4 and Figure 5.5, respectively, there is a difference. It can be seen from the trend lines that the load holds at a high value for some

period around peak load before significant reduction occurs. This 'plateau' region is circled in the figures. The deflection over which this plateau load is held is higher for the five harness Q3DO5 samples (2.5mm) than for the three harness Q3DO3 samples (1mm).

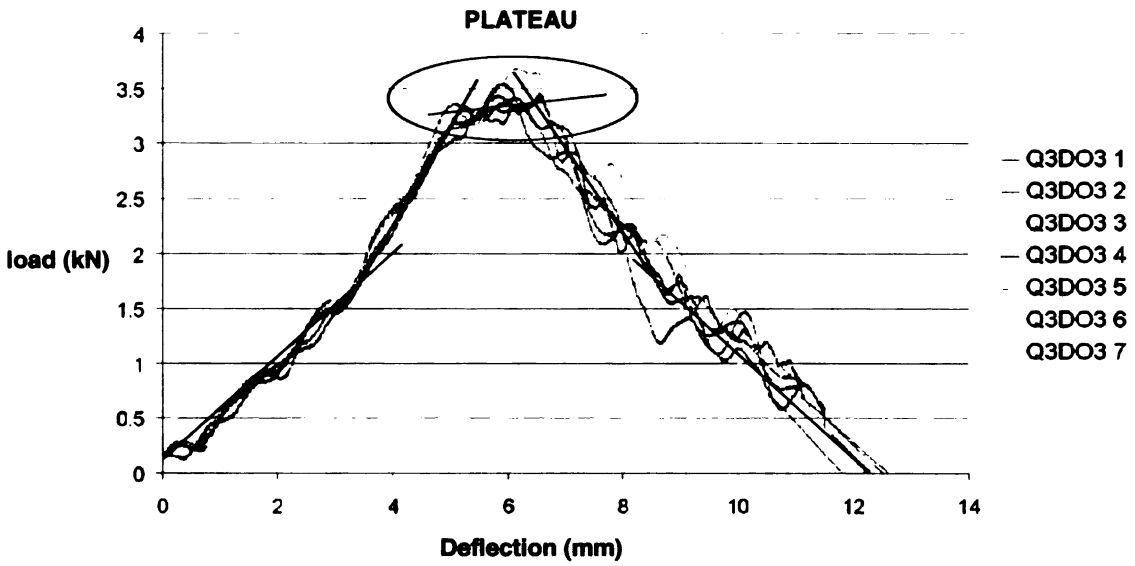

Figure 5.4. Load-deflection curves for Q3DO3 specimen impact tests

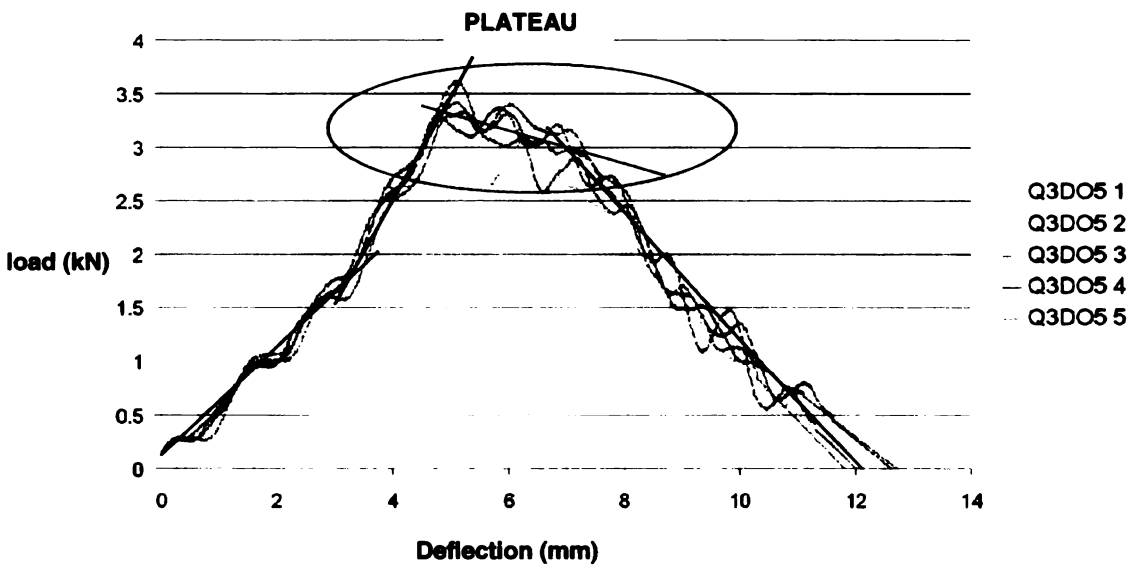

k

Figure 5.5. Load-deflection curves for Q3DO5 specimen impact tests

From the above sets of graphs, one representative plot which best represents each batch (the plot which is most averaged within the group for all

sections of the curve), are used to make the comparison plot shown in Figure 5.6. This is used to contrast the differences between the load-deflection curves of the different sample types as previously explained.

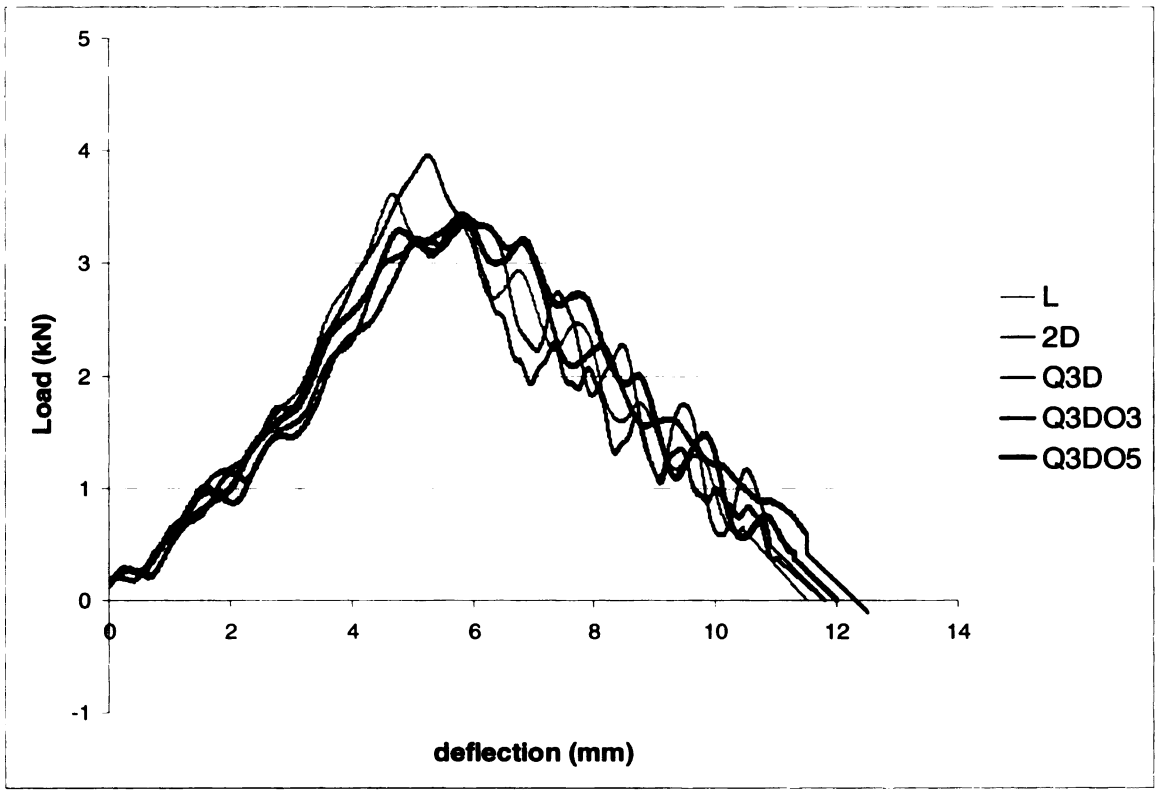

Figure 5.6. Comparison load-deflection curves

The significance of these differences between the load-deflection behavior of the different samples, and how they affect energy absorption and damage resistance will be explained in following chapters.

5.1.2 Impact Characteristics for Thin Specimens

From the above sets of load-deflection curves, several quantities were measured. The method of measuring these different quantities as well as their significance was explained in Chapter 4. Average values of these measured quantities for each group, along with percentage deviations are presented in **Error! Reference source not found.**.

Table 5.1. Impact Characteristics

Sample Group	Thickness mm	Absorbed Energy J	Maximum Load kN	Maximum Deflection mm	Slope1 kN/mm	Primary Damage Area mm^2	Secondary Damage Area mm^2	Specific Energy Absorption mJ/mm^2
L	2.0 ±2%	20.62 ±5%	3.5 ±5%	11.9 ±5%	0.56 ±4%	157 ±5%	718 ±15%	8.5 ±8%
2D	2.1 ±6%	20.10 ±4%	3.6 ±7%	11.7 ±6%	0.52 ±6%	158 ±17%	250 ±26%	9.6 ±14%
Q3D	2.0 ±3%	18.24 ±5%	3.4 ±6%	11.8 ±4%	0.46 ±5%	134 ±8%	280 ±4%	10.4 ±7%
Q3DO3	2.0 ±2%	20.71 ±3%	3.5 ±5%	12.3 ±3%	0.57 ±6%	128 ±12%	399 ±21%	11.4 ±8%
Q3DO5	2.0 ±5%	20.91 ±4%	3.5 ±1%	12.2 ±4%	0.52 ±5%	125 ±4%	428 ±21%	11.6 ±6%

These impact characteristics are presented in graphical form in Figure 5.7. Fiber volume fraction has also been added to this plot. The quantities of greater interest in this study are depicted bolder.

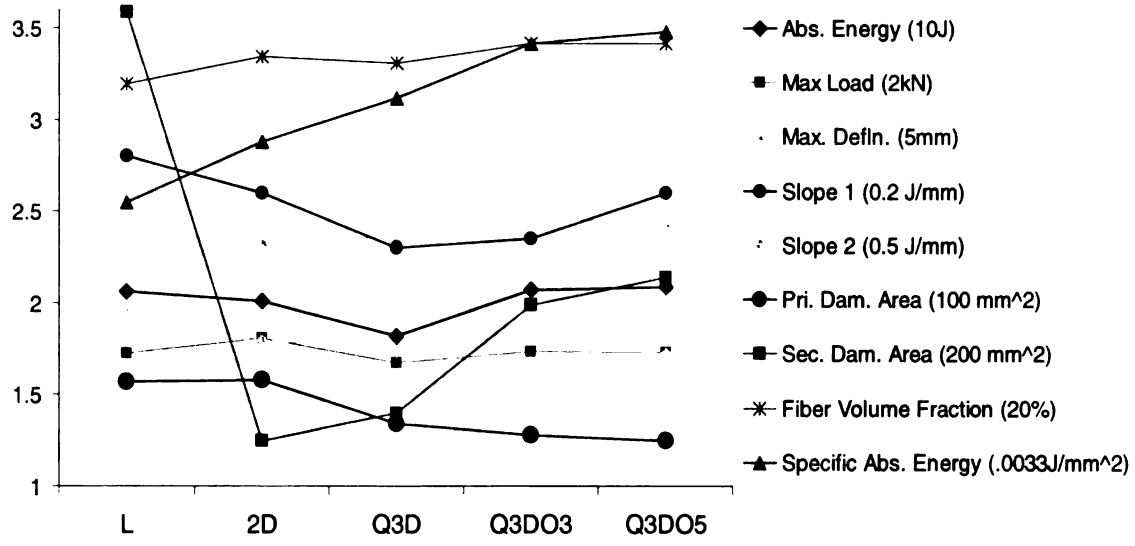

Figure 5.7. Impact Characteristics

5.1.3 Photographs of Impacted Thin Specimens

In this section photographs of impacted specimens for each group, which are most representative of the average damage areas mentioned above, will be

presented. Photographs of all specimens are available in *Appendix 1*. For each sample group, backlit (picture on the left) as well and bottom view photographs (pictures on the right) are presented. From these pictures, extent of *primary* and *secondary damage* areas is observed. Difference in surface finish or texture is also observed in each case.

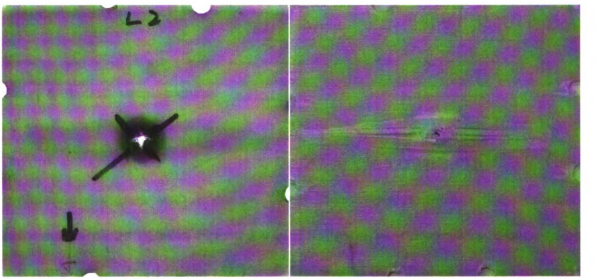

Figure 5.8. L sample pictures

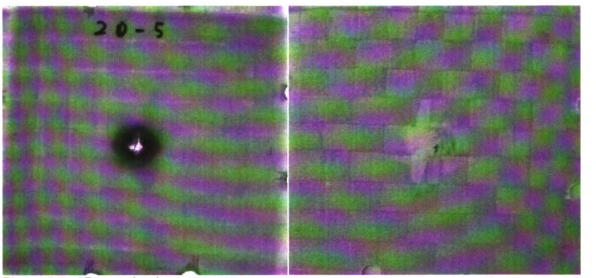

Figure 5.9. 2D sample pictures

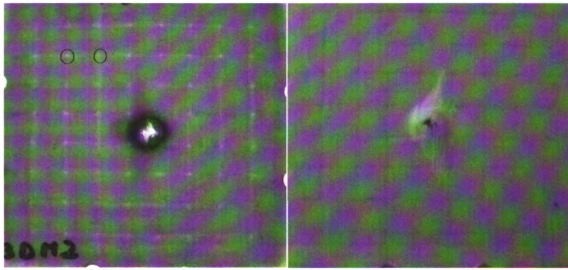

Figure 5.10. Q3D sample pictures

From Figure 5.8, it is noticed that L samples have a flat surface and uniform composition at all cross sections. 2D and, to a greater extent, Q3D have undulating surfaces with lines of higher resin content in the gap between adjacent yarns as seen in Figure 5.9 and Figure 5.10, respectively. These gaps are more pronounced in the Q3D samples due to their higher undulation which causes the weave to be less closely packed. This results in pure resin regions at the corners of the unit cells which are circled in Figure 5.10. It will also be noticed that the *primary damage* area for L and 2D is higher than that of the three dimensionally integrated Q3D weave. The *secondary damage* areas for 2D and Q3D, which are both two harness weaves, are the smallest among the groups. The infinite harness L samples showed unconstrained fiber stripping in the rear surface till the boundaries of the specimen holder, resulting in the largest *secondary damage* area.

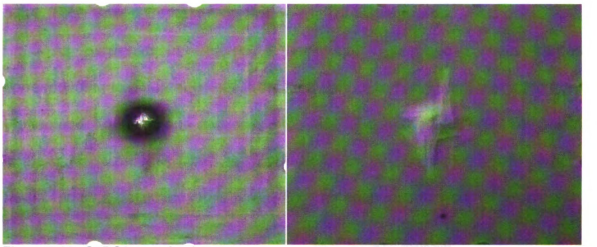

Figure 5.11. Q3DO3 sample pictures

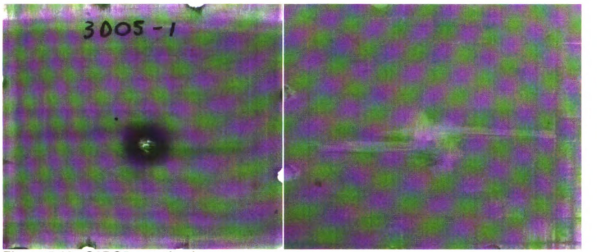

Figure 5.12. Q3DO5 sample pictures

Figure 5.11 and Figure 5.12 show Q3DO3 and Q3DO5 samples respectively. Here the effect of the offset feature becomes clear. In both cases, there are only faint lines at every half-yarn width in the backlit pictures. These are the gaps between adjacent yarns, but they are much less prominent as they are more uniformly distributed, yielding a more homogeneous composition. It is seen that the primary damage areas in both cases are controlled, where as the rear face stripping increases with harness number, with Q3DO5 having the largest constrained *secondary damage* area (its end points are controlled by the cross yarns).

5.1.4 High Speed Camera Correlation for Thin Specimens

As explained in Chapter 4, individual high-speed camera frames corresponding to different points in the load-deflection curve were extracted from the footage. These help to understand the state of damage at different key points in the damage process (like peak load). Following are such high-speed camera frame and load-deflection curve correlations for each sample type.

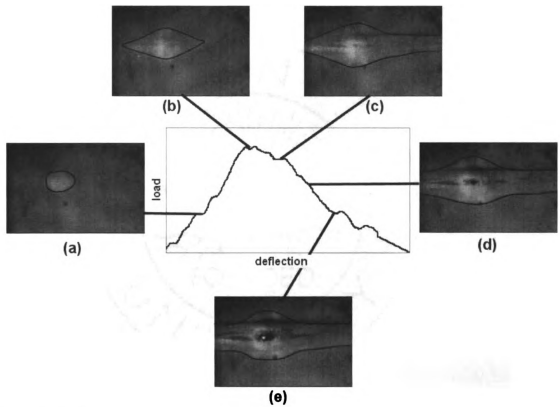

Figure 5.13. Damage sequence in L samples

In Figure 5.13, frame (d) shows a point beyond which there is no increase in damage area, and it occurs in the region of steep descent of the load curve. Similarly, in Figure 5.14, there is no significant increase in the size of damage area (frames (d) and (e)) as the load curve descends after the peak load and similarly in Figure 5.15 frames (d) and (e).

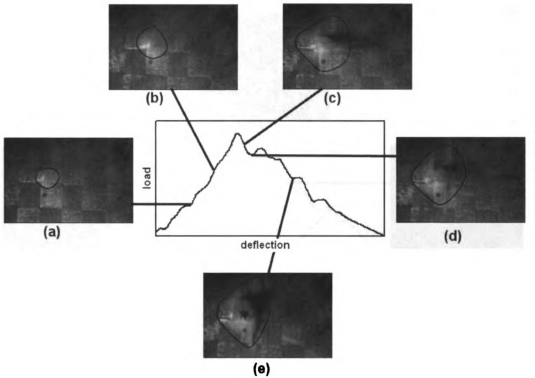

Figure 5.14. Damage sequence in 2D samples

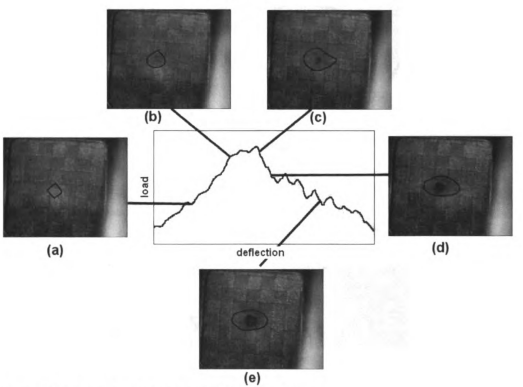

Figure 5.15. Damage sequence in Q3D samples

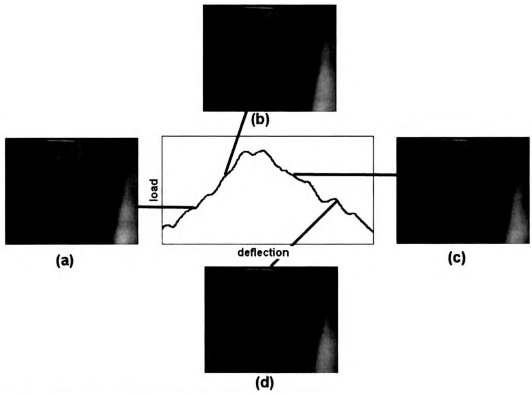

Figure 5.16. Damage sequence in Q3DO3 specimens

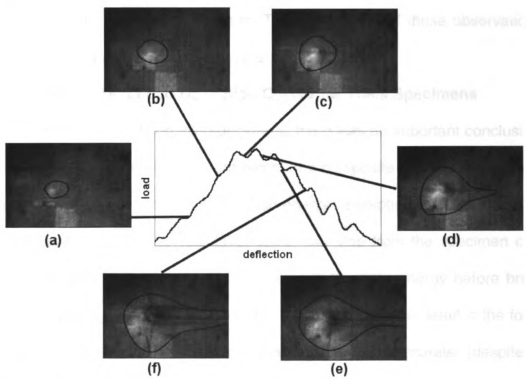

Figure 5.17. Damage sequence for Q3DO5 samples

From Figure 5.17, the behavior of the Q3DO5 weave is seen. The *secondary* damage area continues to grow along the plateau region (frames (c), (d) and (e)) and reaches approximately its maximum when the curve starts to descend more steeply (frame (f)). The performance of Q3DO3 in Figure 5.16 is similar.

It is noted from the above illustrations that the end of slope 1 marks the onset of permanent damage seen as delamination. Also, at the point where the load begins to drop considerably (whether immediately after peak load, or after a short 'plateau' region), *secondary* damage has reached its maximum. From the beginning of slope 2 till the load begins its decline, the damage area (both *primary* and *secondary*) grows in size. After this point of maximum *secondary* damage and start of load decline, the tup pushes its way through the specimen, without further measurable damage. The significance of these observations will be discussed in the following chapters.

5.1.5 Impact Test Load-Deflection Curves for Thick Specimens

From the study on thin specimens, there was an important conclusion that was drawn. This was that the rear layers of a composite plate (especially the last layer) have a more prominent effect on energy absorption than the other layers. This was because these rear layer yarns can strip from the specimen creating longer lengths of free yarns which take up high strain energy before breaking, especially in high harness weaves (this will be explained in detail in the following chapters). To verify that the concept was in fact accurate (despite small variations in specimen thicknesses), and to verify that it was accurate in thicker

specimens, a study was conducted on thicker 6mm specimens. The manufacturing of these specimens had been described in Chapter 3.

As usual, conventional samples of Th L and Th 2D were created as control references. The 'Th' before the nomenclature represents 'Thick'. The most promising weave from the thin sample study, and also the weave with the greatest potential to isolate this rear surface behavior, was the five harness Q3DO5 weave. Samples were produced of this weave (Th Q3DO5 $[0/90]_{12}$) and also a modified version of it designated as Q3DO5 X (Q3DO5 X $[(0/90)_8/(0_2/90_2)_2]$. In the modified version, the same number of yarns were used to build up the thickness, but the last four layers were formed into just two layers, with each layer being of double thickness. This means that yarns of double thickness were used to weave the last two layers, which were equal in fiber content and thickness to the last four layers of the regular Th Q3DO5 weave.

The reason for doing this was so that when the rear layer of the Q3DO5 X specimen stripped from the specimen and went into high tension before breaking, there would be double yarns to take up strain energy. If in fact, this tensile straining was a high energy absorber, the energy absorption in impact of Q3DO5 X would be noticeably higher than that of Q3DO5.

Figure 5.18, Figure 5.19, Figure 5.20 and Figure 5.21 show the load deflection curve groups for Th L, Th 2D, Th Q3DO5 and Q3DO5 X (Th designates thick specimens).

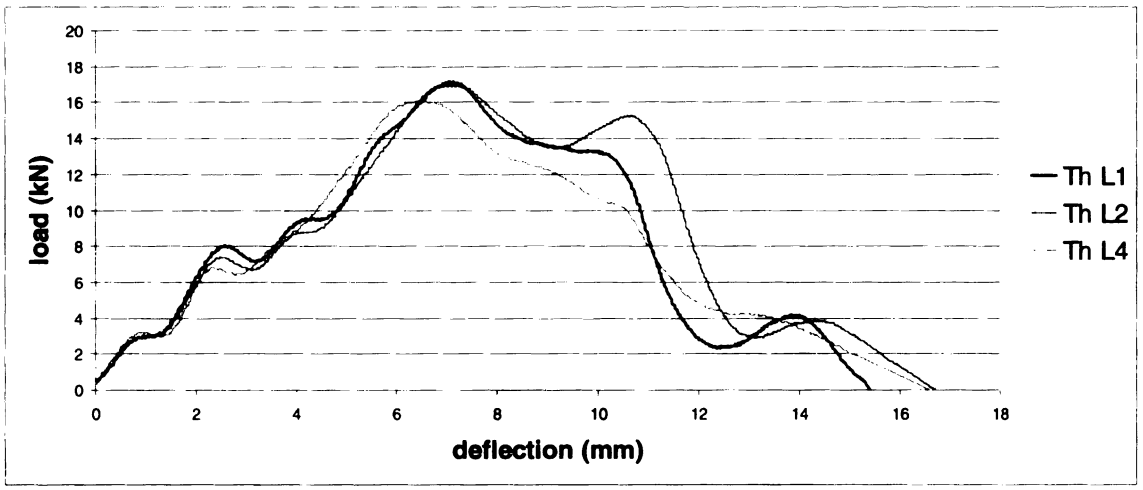

Figure 5.18. Load-deflection curves for Th L specimen impact tests

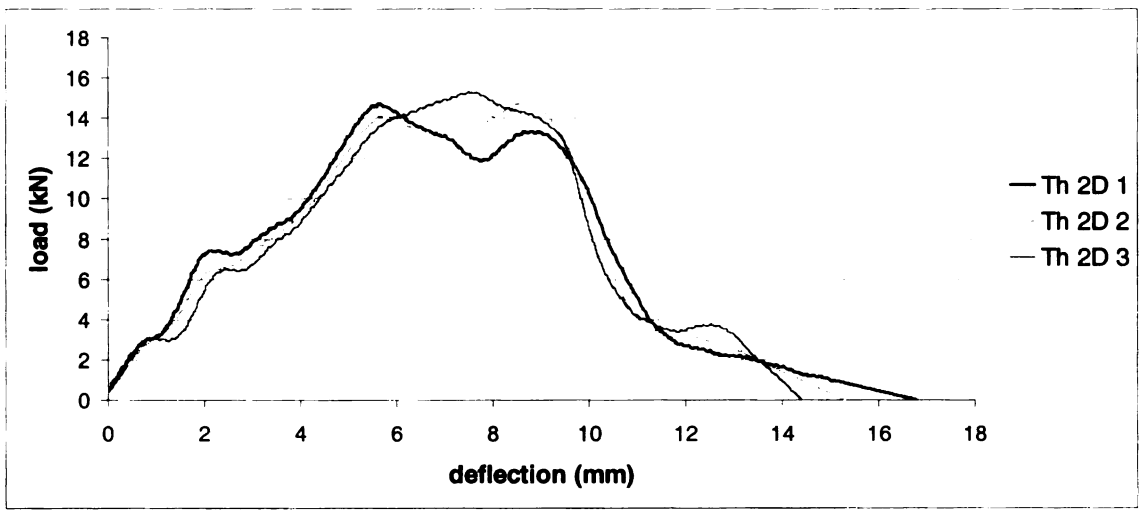

Figure 5.19. Load-deflection curves for Th 2D specimen impact tests

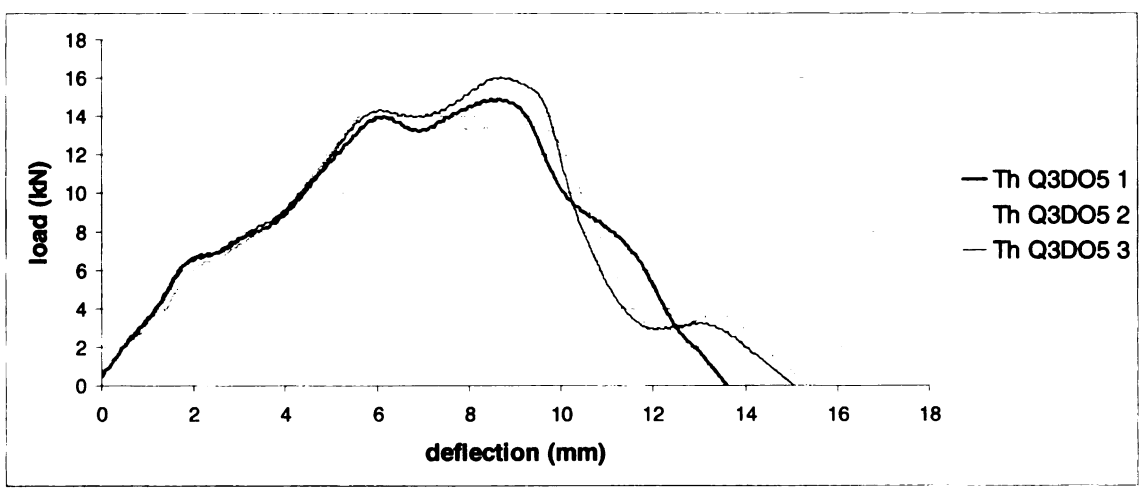

Figure 5.20. Load-deflection curves for Th Q3DO5 specimens

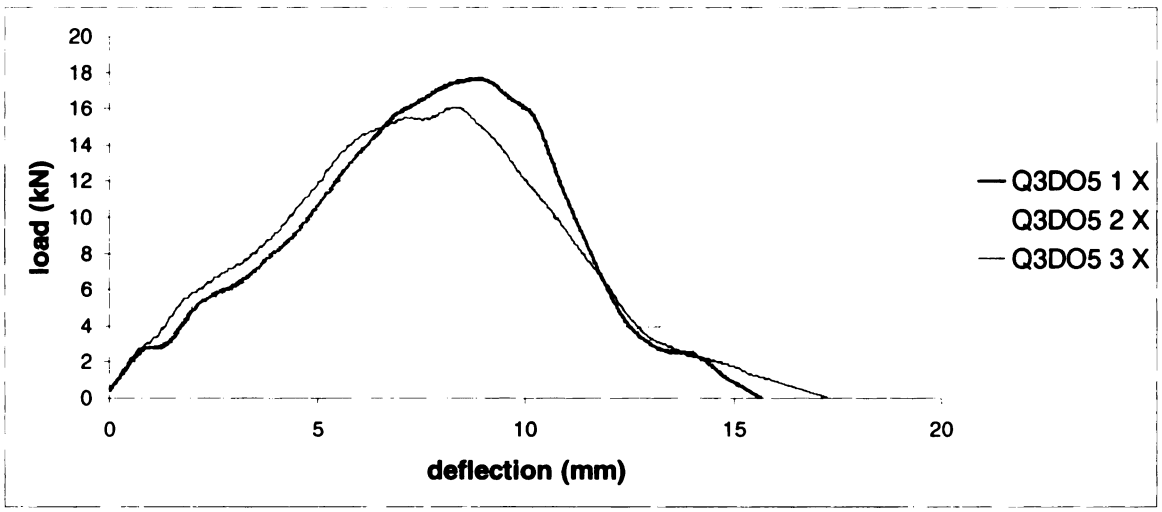

Figure 5.21. Load-deflection curves for Q3DO5 X specimen impact tests

From these plots, a composite comparison plot is drawn using the most generalized curves from each group. This is shown in Figure 5.22.

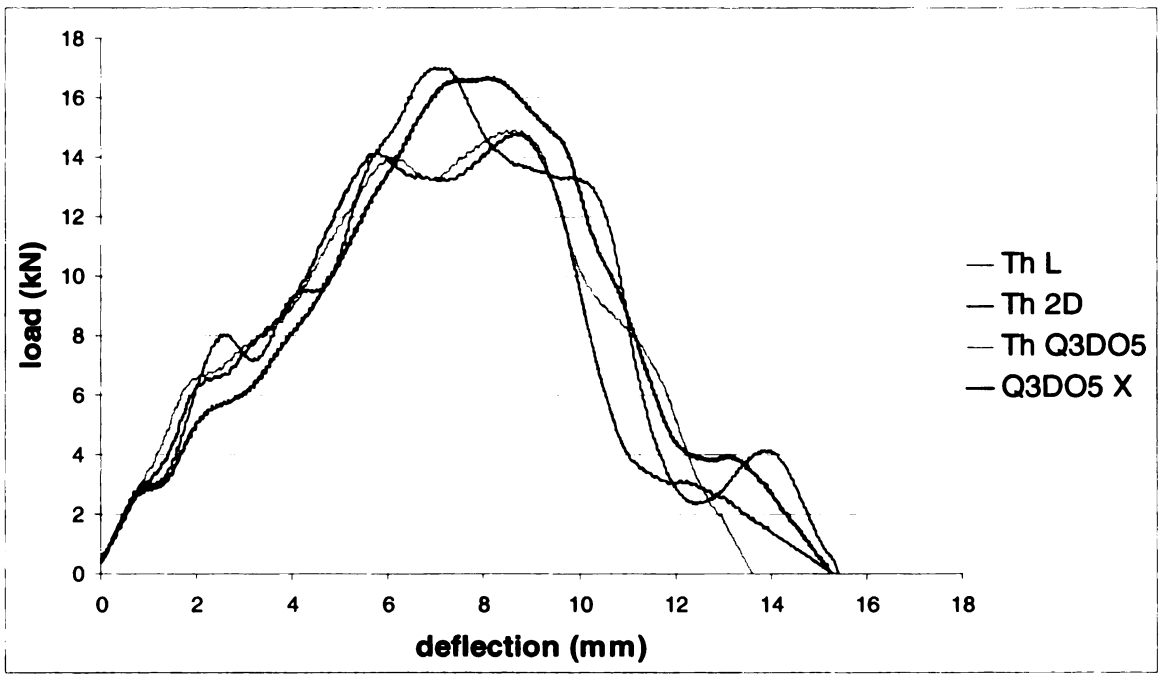

Figure 5.22. Comparison plots from thick specimen study

From the above plots the following important impact characteristics are measured shown in **Error! Reference source not found.**. These are shown in graphical form in Figure 5.23.

Table 5.2. Impact characteristics for thick specimen study

SPECIMEN	Absorbed Energy (J)	Maximum Load (kN)
Th L	133.74 ±6%	16.76 ±3%
Th 2D	115.62 ±1%	14.93 ±2%
Th Q3DO5	122.69 ±2%	15.36 ±4%
Q3DO5 X	132.56 ±3%	16.89 ±5%

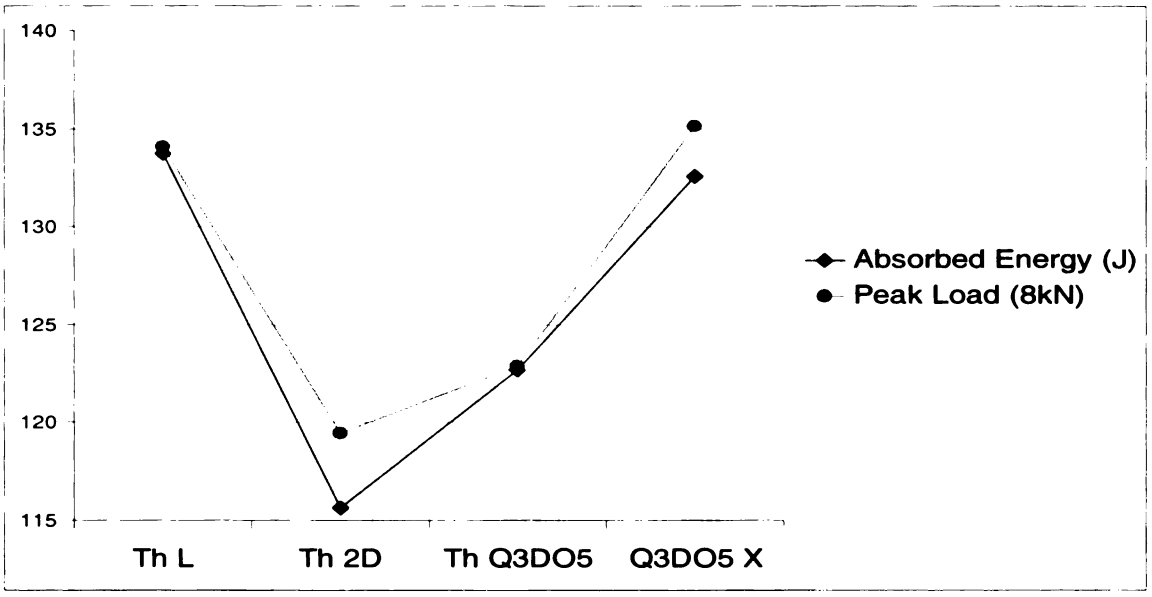

Figure 5.23. Impact characteristics plot for thick specimen study

From the above study on thick specimens, the following observations are made: Th Q3DO5 specimens performed better than Th 2D specimens for impact energy absorption, but not as well as Th L samples. This is in comparison to the study on thin specimens where Q3DO5 slightly outperformed even L samples. This will be explained in later chapters as being due to the effect of rearmost fiber straining in thin specimens being more prominent due to lower number of layers overall. However, it is seen in the Q3DO5 X specimens, where the effect of rearmosy layer straining was exaggerated by doubling its thickness, energy

absorption was considerably higher (7.8%) than Th Q3DO5, and matched up well to Th L absorbed energies.

5.2 Compression Tests for Thin Specimens

5.2.1 Load-Deflection Curves

Following are the load-deflection curve groups for the five groups of thin specimens subjected to compression tests. They are presented to show the variation within each set, and the general trends in each case. Some of the sample sets start with D in their nomenclature. This is short for 'damaged' and represents specimens which were put through compressive testing after being damaged by penetration. The plots for these samples are in dashed lines. Samples without the prefix D are undamaged specimens that were put through compression tests. Plots for these are in solid lines.

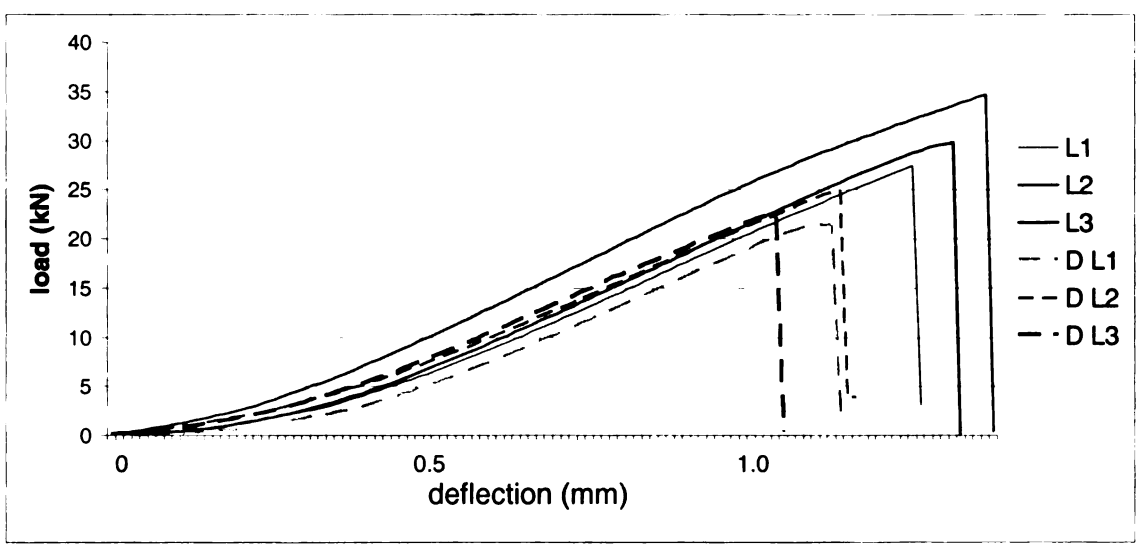

Figure 5.24. Load-deflection curves for L sample compression tests

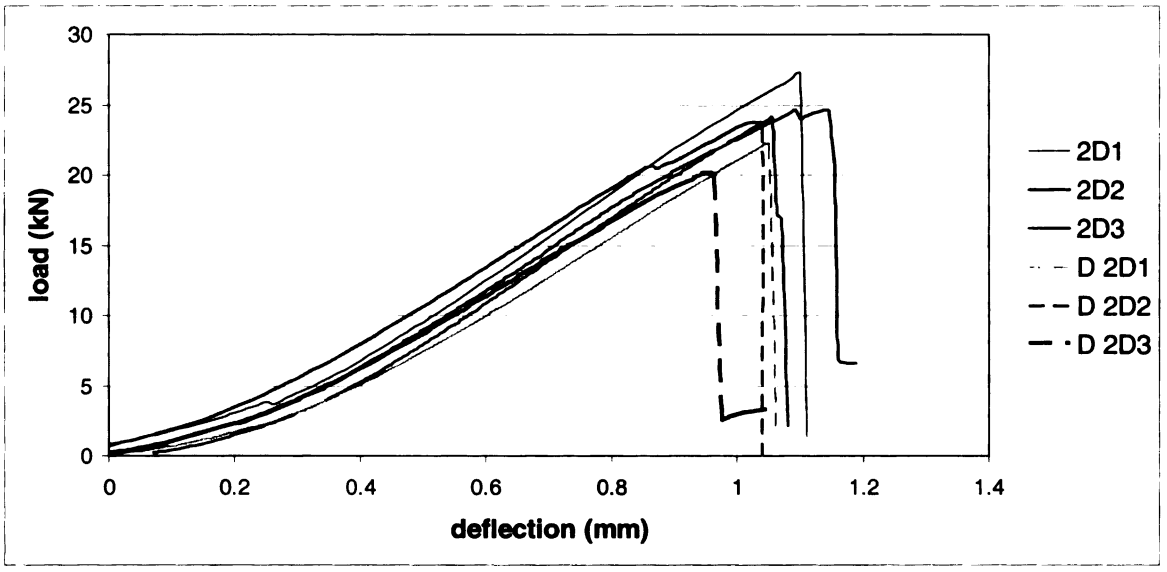

Figure 5.25. Load-deflection curves for 2D sample compression tests

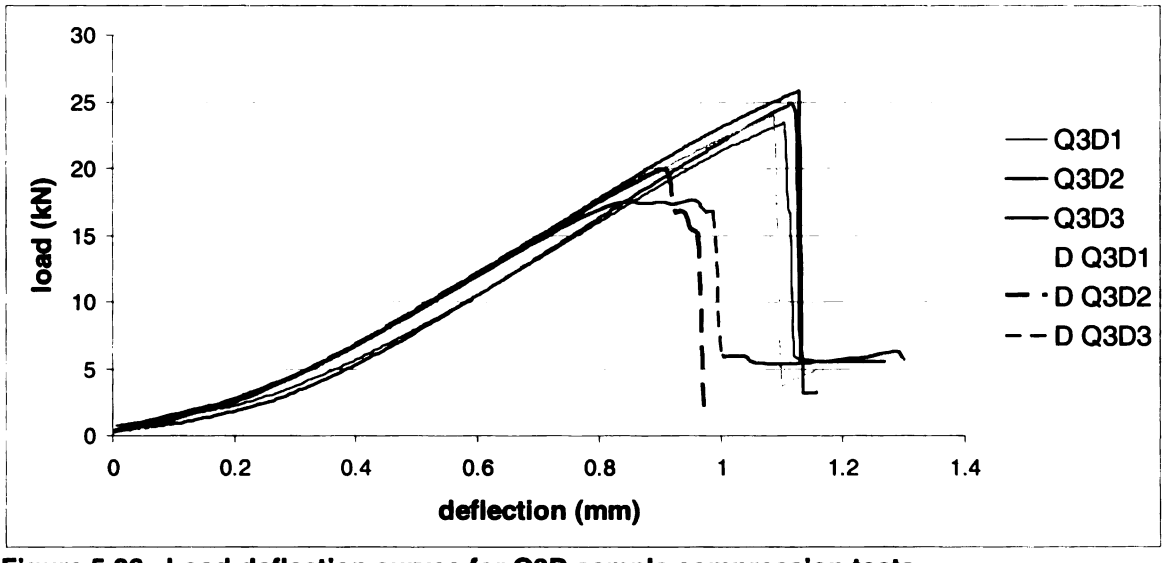

Figure 5.26. Load-deflection curves for Q3D sample compression tests

Figure 5.24, Figure 5.25, Figure 5.26, Figure 5.27 and Figure 5.28 show the load-deflection curves for L, 2D, Q3D, Q3DO3 and Q3DO5 weaves respectively. It can be seen in all cases that in general, penetrative impact reduces the load bearing capacity of the specimen. It is less apparent from the plots that there is also a loss in stiffness as a result of impact damage. This will be clearer when the measured values are presented shortly. In this study,

measured values were normalized with the specimen thickness as explained in earlier chapters, to accommodate any differences in thickness of samples.

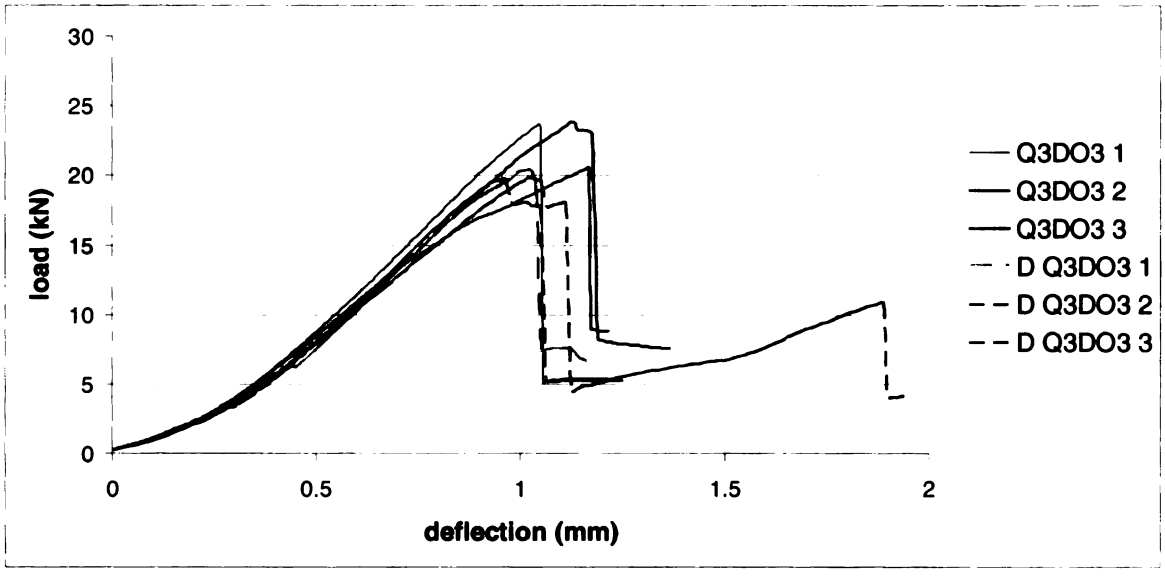

Figure 5.27. Load-deflection curves for Q3DO3 sample compression tests

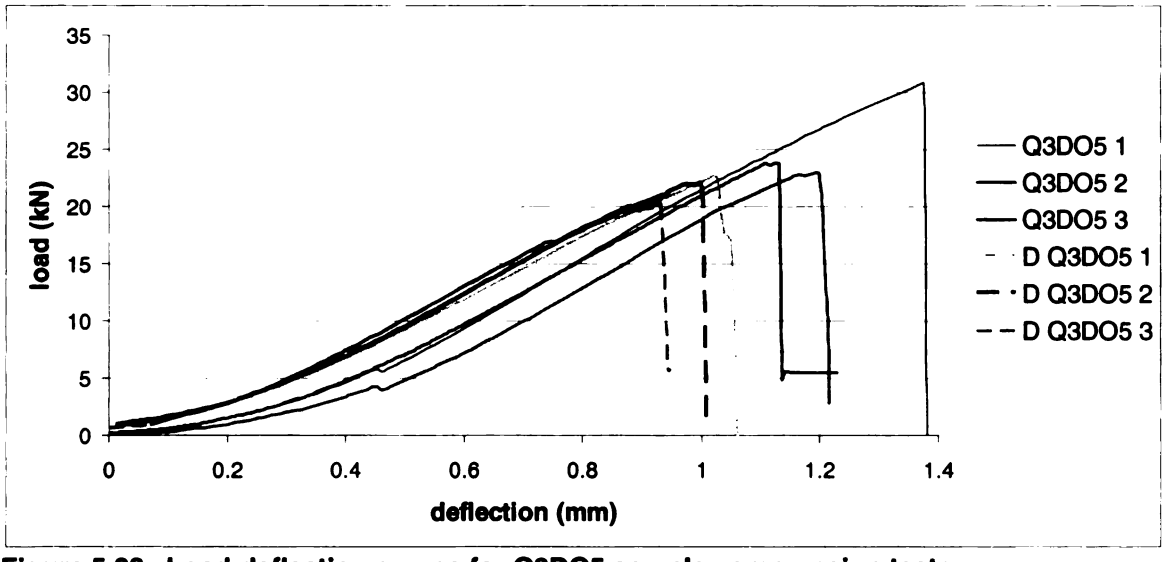

Figure 5.28. Load-deflection curves for Q3DO5 sample compression tests

From Figure 5.24, it is seen that in general, L samples lose all or most of their load-bearing ability when they fail due to compression, seen as a sudden drop in load to zero or near zero. This is also seen in most cases in 2D and Q3DO5. It should be noted here that for the tests in which the load drops very

suddenly to near zero, the testing machine automatically cuts off and retracts when it senses a large drop in load. This is an inbuilt safety feature which signals the end of the test. The drop portion of the plot occurs in sometimes one or two data recording points. Thus it is very likely that in the plots where the load drops suddenly to a finite value near zero, the final load value might be even lower, but the machine cut off before the next data point was recorded.

However, in the smaller harness Quasi-three-dimensional weaves (Q3D and Q3DO3), it is seen that in several cases, the load would not drop down to near zero. It would reach a certain low value, but still resist complete failure. The damage process was also different from the former three cases (L,2D and Q3DO5) in that the specimen would buckle instead of failing by shear. This will be described shortly. When this type of response occurred, the testing fixture tended to go out of alignment, so most tests were manually ended after the first breach in structural integrity (first big drop in load) to prevent damage to the fixture. However, as can be seen from Figure 5.27, one test was prolonged past the first loss in load-bearing ability, to see how the specimen would finally fail. This is sample D Q3DO3 3. The load curve rose for a second time and then dropped suddenly again, still without dropping to zero, but seemingly continuing at that load. At this point, the test was terminated for safety and care of the fixture. The made of failure is described shortly.

5.2.2 Compression Characteristics

Before further presentations of these damage modes, the compression characteristics that were measured from the above plots are presented in **Error!**

Reference source not found.. These characteristics are again presented in Figure 5.29 in graphical form. As before, the quantities of interest are plotted in bold. The values presented have been thickness normalized. Percentage deviations are also presented.

Table 5.3. Compression characteristics for thin specimens

Sample	Peak Load Undamaged (kN/mm)	Peak Load Damaged (kN/mm)	Stiffness Undamaged (kN/mm^2)	Stiffness Damaged (kN/mm^2)	% Reduction in Load	% Reduction in Stiffness
L	13.91 ±14%	10.68 ±6%	13.80 ±4%	12.62 ±3%	23.2	8.5
2D	12.34 ±7%	10.08 ±3%	13.63 ±1%	12.19 ±4%	18.3	10.6
Q3D	12.06 ±6%	10.17 ±13%	13.31 ±6%	12.85 ±1%	15.7	3.4
Q3DO3	12.06 ±2%	10.01 ±2%	13.48 ±7%	12.76 ±1%	17.0	5.3
Q3DO5	12.59 ±13%	10.45 ±8%	13.62 ±7%	12.67 ±1%	16.9	6.9

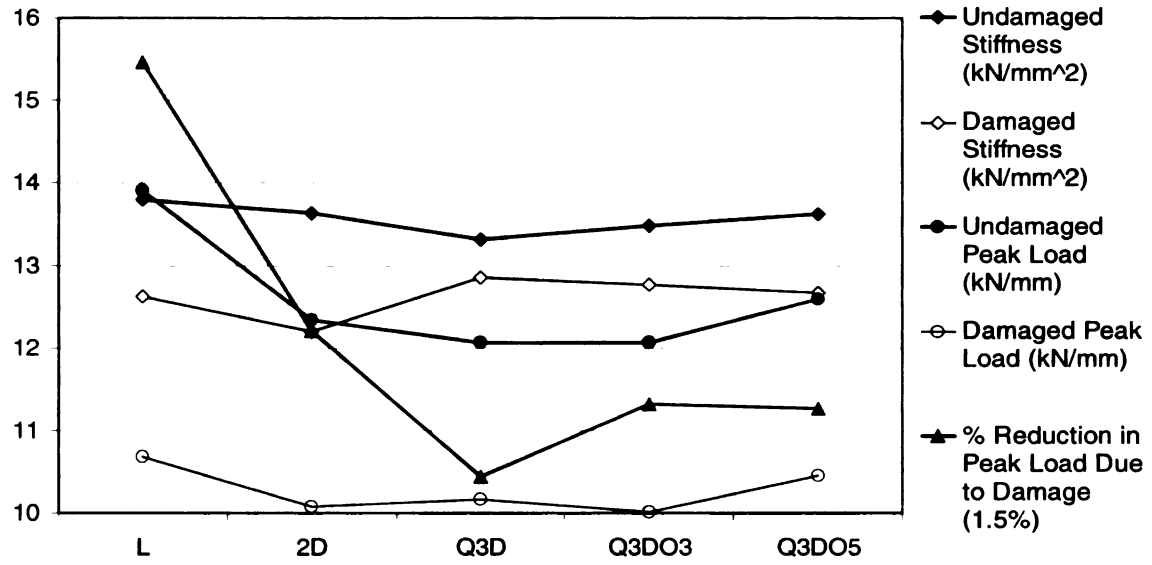

Figure 5.29. Compression characteristics for thin specimens

From Figure 5.29, the quantities that clearly differentiate the different sample groups are the undamaged peak load, and the percentage loss in load-bearing ability due to damage. Q3DO5 weave is seen to out-perform 2D in peak load, while having stiffness similar to 2D as was seen in the impact tests. It is

apparent that quasi-three-dimensional weaves lose less of their load-bearing ability due to inflicted damage. Although it might be said that Q3D and Q3DO3 weaves started out having a lower undamaged peak load, and thus they would show lower reduction. This is true. However, the Q3DO5 weave again proves to be a good configuration as it had an undamaged peak load higher than 2D and similarly with damaged peak load. So in its case, the lower percentage load loss is truly indicative of an advantage.

5.2.3 Compression Test Specimen Photographs and Damage Patterns

In this section backlit photographs of compressed specimens for each group, which are most representative of the damage pattern and mode for that group, will be presented. Backlighting makes the damage pattern (seen as darker regions) more clear. Photographs of all specimens are available in *Appendix 2.*

As explained earlier, there were two different types of failure in the compression test specimens. One was shear failure and one was bending failure. L, 2D and Q3DO5 groups were dominated by shear failure, while in the small harness quasi-three-dimensional weaves, Q3D and Q3DO3, there was general occurrence of buckling failure.

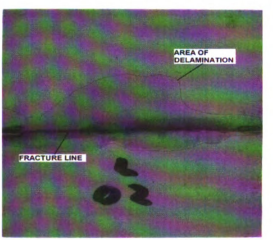

Figure 5.30. Compressed L sample

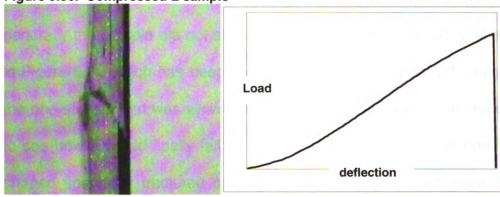

Figure 5.31. Shear damage and corresponding load-deflection curve

Figure 5.30 shows an L sample with shear damage while Figure 5.31 shows the side view of the damaged section. A clear fracture line is seen along which the specimen sheared, sometimes into two pieces. Similarly, Figure 5.32 and Figure 5.33 show shear damage in 2D and Q3DO5 specimens respectively.

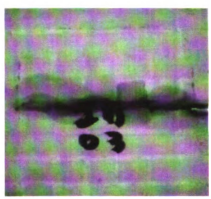

Figure 5.32. Compressed 2D sample

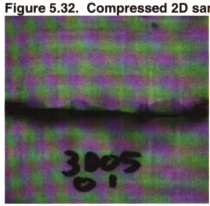

Figure 5.33. Compressed Q3DO5 sample

In the case of Q3D and Q3DO3 specimens, at the first point of failure, in generally the sample did not shear, but rather buckled into an 's' shape as seen in Figure 5.34 which has been correlated with the load-deflection curve. This is the one sample that was allowed to be compressed beyond the first drop in load to see how it would finally fail. When the load dropped the second time, the 's' shaped specimen fractured on one side at the two fixture support points as shown. The other side of the sample still maintained this 's' shaped, holding the residual load.

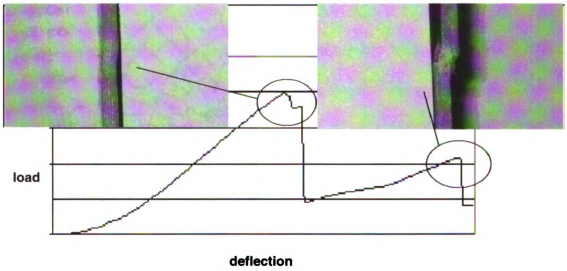

Figure 5.34. Buckling damage

This acute bending would no doubt cause large scale delamination in a specimen. From the Q3D and Q3DO3 damage specimens shown in Figure 5.35 and Figure 5.36 respectively, it is seen that even though the delamination is severe, it is contained within the dimensions of the weave's unit cell (one yarn width for Q3D and two yarns width for Q3DO3). Discussions on these damage patterns and their significance will be presented in the next chapter.

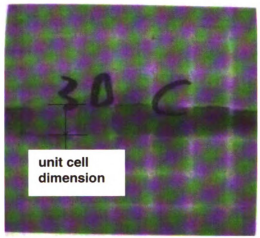

Figure 5.35. Compressed Q3D sample

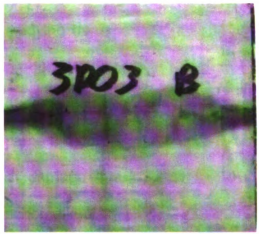

Figure 5.36. Compressed Q3DO3 sample

CHAPTER 6

Discussions

In this chapter, the relevance of the results presented in Chapter 5 will be discussed in an attempt to extract useful conclusions regarding how quasi-three-dimensional weaves fare in relation to traditional weaves.

6.1 Impact Damage Modes

The impact tests that were run on thin specimens proved useful in studying damage processes in the different weave sets, as they were easy to produce, they were thin enough to be inspected for damage using a light table, and their reaction to impact could be adequately studied using a high-speed camera recording the rear face of the specimen. There was a general sequence of damage that was noticed in all the thin specimens. Figure 6.1 shows a schematic of this sequence.

Along the region of *slope 1* in the load-deflection curves (described in Figure 4.3), the specimen was in global elastic bending. During this period, damage had not yet begun. The point of intersection of *slope1* and *slope 2* (Figures 4.3) marked the onset of visible local damage in the form of local matrix crushing under the spherical tip of the tup, which showed through the specimen to its bottom surface due to its low thickness. This is best represented by Figure 6.1 (a). The entire *slope 2* region marked the period of visible damage growth in the form of delamination caused by bending and the pushing of the upper crushed layers, as seen in Figure 6.1 (b), which was most prominent along

the rear face of the specimen. The load values increased till peak load was reached. In cases where there was a plateau region (Q3DO3 and Q3DO5), the visible damage along the rear face reached a maximum at the end of the plateau region.

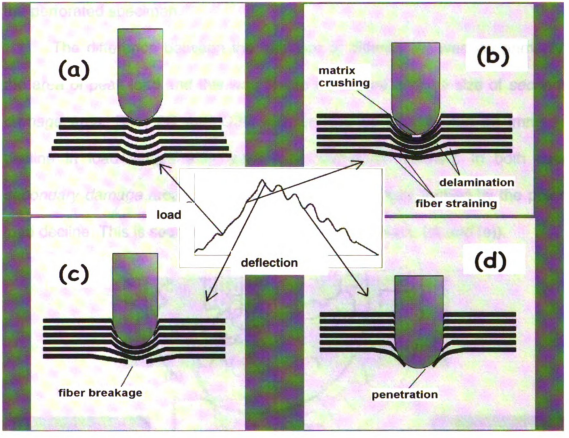

Figure 6.1. Damage sequence for thin specimens

In all cases, the beginning point of descent of the load curve (whether it be immediately after peak load or after a plateau region), marked the point when the maximum visible *secondary damage* was reached. Beyond this point, fiber breakage began from the rear layer upwards and the tup proceeded to perforate the specimen. This is in agreement with work of other authors who found that stiff plates tend to have damage progression from front to back caused by contact stresses. Plates that were less stiff (as in this study) had damage progressions

from back to front as a result of flexural stresses [12]. The upper layers which had undergone crushing failed by shearing while the rest failed by tensile straining. This led to consecutive weakening of the section, hence the decline in load values. This step is represented in Figure 6.1 (c). Figure 6.1 (d) represents the perforated specimen.

The difference between the behavior of different weaves lay primarily in the area of peak load and this was tied to the nature and the size of *secondary damage* area. Both 2D and Q3D weaves had no plateau, but an immediate decline in load values after peak load had been reached. In both cases, *secondary damage* area was small and was almost fully formed by the point of load decline. This is seen for 2D in Figure 6.2. (frames (c), (d) and (e)).

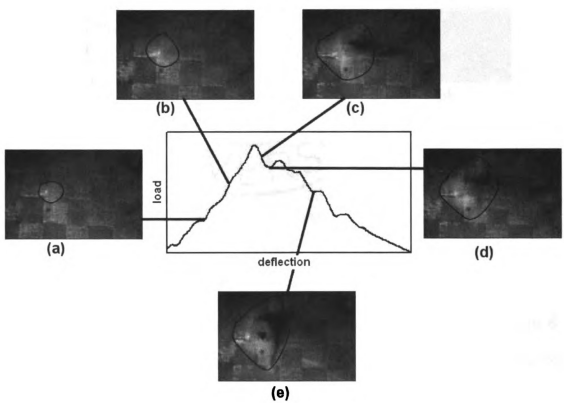

Figure 6.2. Damage sequence in 2D specimens

Laminated (L) samples too had a decline in load after peak load was reached. However, it seems from Figure 6.3 (from frames (c) and (d)) that the *secondary damage* area is still growing after this point. In fact it is, but the rear layer which is stripping from the specimen (Mode 1 peeling), is unconstrained and is thus too loose to offer much resistance. After a point, these fibers are so free from the rear surface of the specimen that they split apart from each other, and the tup passes through them instead of breaking them (frame (e).

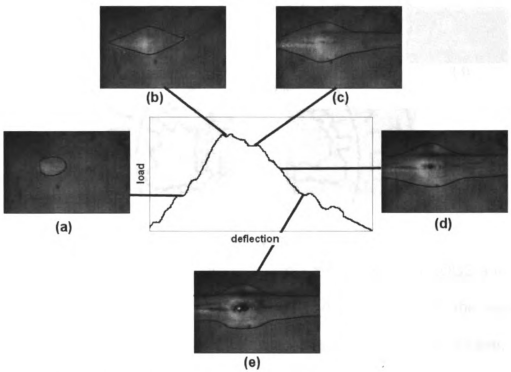

Figure 6.3. Damage sequence for L specimens

From the damage sequence of the Q3DO5 weave shown in Figure 6.4, the behavior of it and Q3DO3 can be understood. It is seen that the *secondary damage* area continues to grow (frames (c), (d) and (e)) until the end of the plateau region (corresponding to 1.5 mm deflection in Q3DO3 and 2.5 mm

deflection in Q3DO5 specimens as seen in Figure 5.4 and Figure 5.5 respectively). It seems that there is some link between this increasing *secondary damage* area and the sustained high loads until it has reached a maximum.

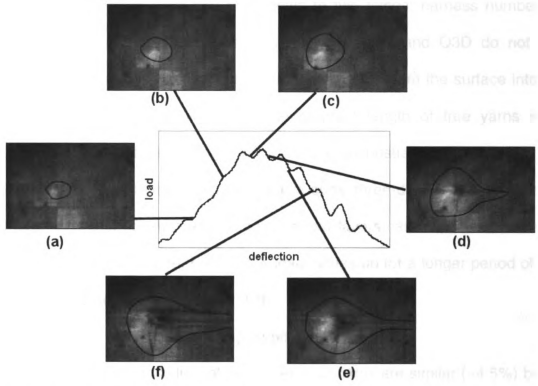

Figure 6.4. Damage sequence in Q3DO5 specimens

The key is that the rear layer in the three-harness Q3DO3 and the five-harness Q3DO5 specimens, although more free to strip from the rear surface (due to higher harness number), is still constrained by the cross weave, and able to offer some resistance. When the tup nears the rear layer, it pulls longer lengths of rear layer tows into high tension (as seen in Figure 6.1 (b)), which maintains the plateau region around peak load, instead of letting the load decline immediately after peak load. It is very likely that the perforation of the upper layers (by shear) has already begun by the time this rear layer has been tensioned completely, corresponding to the similar point of load decline in

specimens like 2D and Q3D. This would explain the slight drop in load in Q3DO5 specimens during the plateau.

So the existence of a plateau region is greatly dependent on the weave structure in the rear layer and boils down to two things: harness number and integration. Small harness numbers like those in 2D and Q3D do not have sufficient free lengths of yarn in the rear layer to strip from the surface into high tension. Although L samples have the greatest length of free yarns in the rearmost layer to take up high tension, it is unconstrained and cannot offer additional resistive force. In higher harness quasi-three-dimensional weaves, the longer lengths of constrained yarns in the rear layers can strip from the surface into high tension to failure, holding the load values up for a longer period of time, which contributes to energy absorption.

6.2 Rear-Layer Fiber Straining Hypothesis

As the strain to failure of both fiber and matrix are similar (~4.5%) but the fiber modulus is much greater than that of the matrix (~22 times greater), strain to failure of fiber would absorb ~22 times the energy as matrix. Also, strain energy taken up by a fiber in tension is proportional to its length. Lee *et al* [29] found that fiber straining is responsible for most of the energy absorption in penetration failure of textile fabrics and fabric-reinforced composites.

It is hypothesized that strain to failure of different lengths of constrained rear-layer fibers in high-harness quasi-three-dimensional weaves is the factor that enables them to maintain plateau regions in load-deflection curves around peak load. This allowed the Q3DO3 and Q3DO5 weaves to outperform both L

and 2D weaves in energy absorption, even though they had a smaller primary damage areas than the latter.

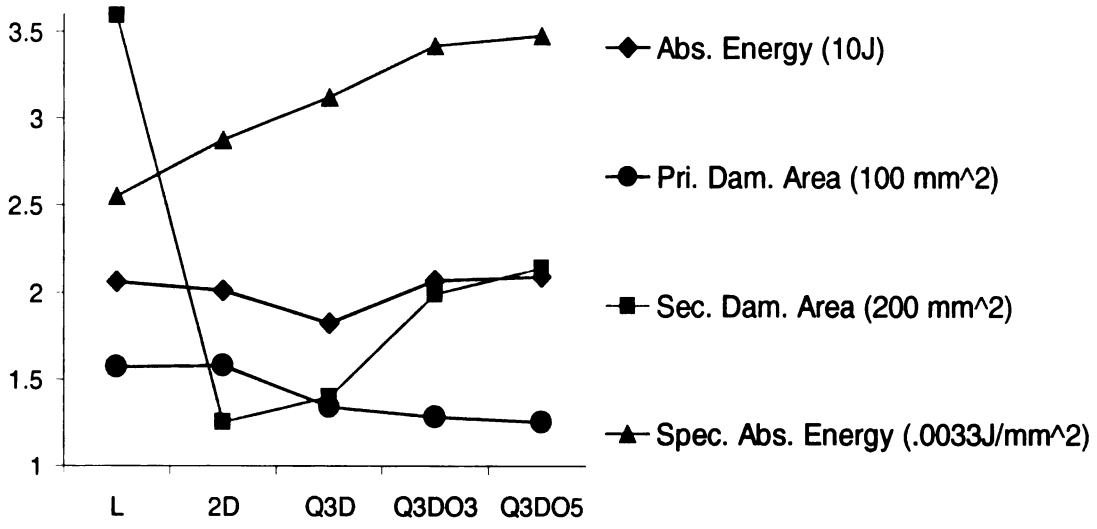

Figure 6.5. Effect of damage area on SEA

This relation is clearly seen in Figure 6.5 where *primary damage* areas of quasi-three-dimensional weaves are all smaller than the conventional weaves (which would lead to lower energy absorption due to lower delamination energy absorption and lower fiber straining). However, it is clear to see how that, with an increase in *secondary damage* area in Q3DO3 and Q3DO5, the energy absorption also increases. Small *primary* and *secondary damage* areas explain the low energy absorption of the two-harness Q3D weave. It can also be seen that the effect of the huge *secondary damage* area did little for the energy absorption as compared to 2D which had similar *primary damage* area but much smaller *secondary damage* area. This is due to the fact that the rear-layer was unconstrained.

As specific energy absorption (SEA) takes into account both primary and secondary damage areas, it is seen that the quasi-three-dimensional weaves have higher values than the conventional weaves, which gets better with increase in harness number.

If the above stated *hypothesis* was true, two things would show up in the tests run on thicker specimens. Firstly, as the effect of rear-layer fiber straining would be less conspicuous in specimens with more layers, its perceived advantage in increasing energy absorption would be reduced in Th Q3DO5 specimens. Secondly, if rear layer fiber straining were a prominent energy absorption mechanism, the Q3DO5 X specimens (which were woven to have thicker rear layers while still maintaining the same fiber content as Th Q3DO5) would have a considerably higher energy absorption than the regular woven Th Q3DO5 specimens.

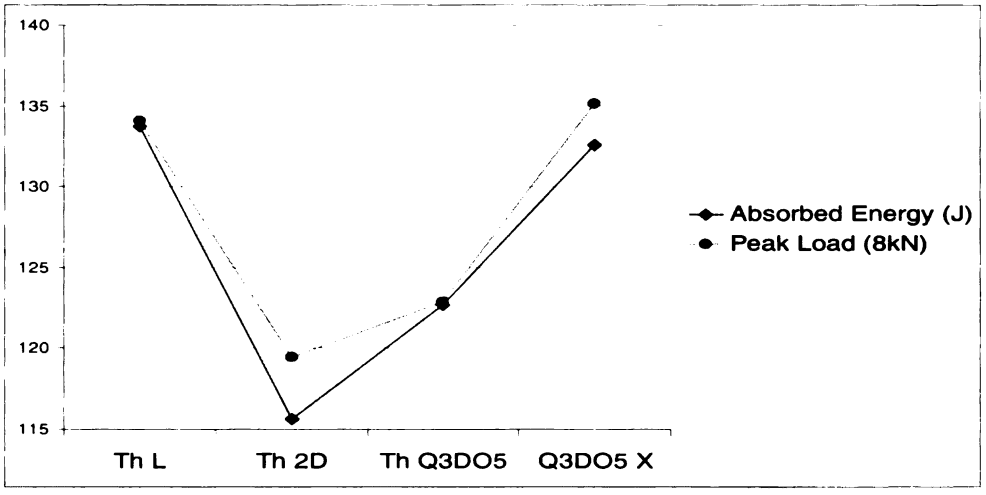

Figure 6.6. Impact characteristics for thick specimens in impact

As seen in Figure 6.6, the Th Q3DO5 specimens could no longer match the energy absorption of the L specimens (although it still did manage to surpass

that of 2D). This is because the energy absorbing advantage from its rear layer was of less consequence in a thick specimen. It is also clearly seen how the modification to increase fiber content in the rear layer (in Q3DO5 X samples) increased energy absorption by a marked 7.8%. These tests prove that strain to failure of longer lengths of constrained rear-layer fibers contributes to higher energy absorption.

6.3 Structural Properties

The two important structural properties that were measured in this study on thin specimens were stiffness and load-bearing ability.

6.3.1 Stiffness

From the impact tests, *slope 1* corresponds to the global bending stiffness of the specimen. This stiffness is dependent on the in-plane undulation of the weaves. The greater the undulation, the lower is the stiffness. Thus this value is a good measure of the overall extent of undulation in the weave.

In this study, flat wide tows were used instead of conventional eye-shaped tows for two reasons, which are illustrated in Figure 6.7. Firstly, resin pockets (which are weak points and areas of damage initiation) tend to be larger with eye-shaped tows. More importantly, the aim of quasi-three-dimensional weaving was to have each yarn contribute as much as possible to in-plane properties. This would be achieved by reducing the undulation in the yarns to a minimum to try to be as close to the L configuration (which has the maximum efficiency of fiber load bearing).

As can be seen in Figure 6.7 (a), thinner layers result in lower undulation. Also it is known that because delamination is caused by a bending stiffness mismatch between adjacent plies in the layup, the thinner each ply is, the lower the tendency to delaminate [1]. It was seen from the edge replications in Chapter 3 that the undulation angles for all weaves are very small with none exceeding 10°.

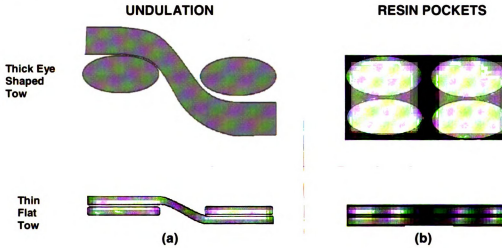

Figure 6.7. Demonstration of undulation

Compressive stiffness was also measured in the compression tests. These are similarly dependent on the undulation of the weaves. Figure 6. shows the stiffness values measured from slope 1 of the impact tests, and the normalized compressive stiffness values.

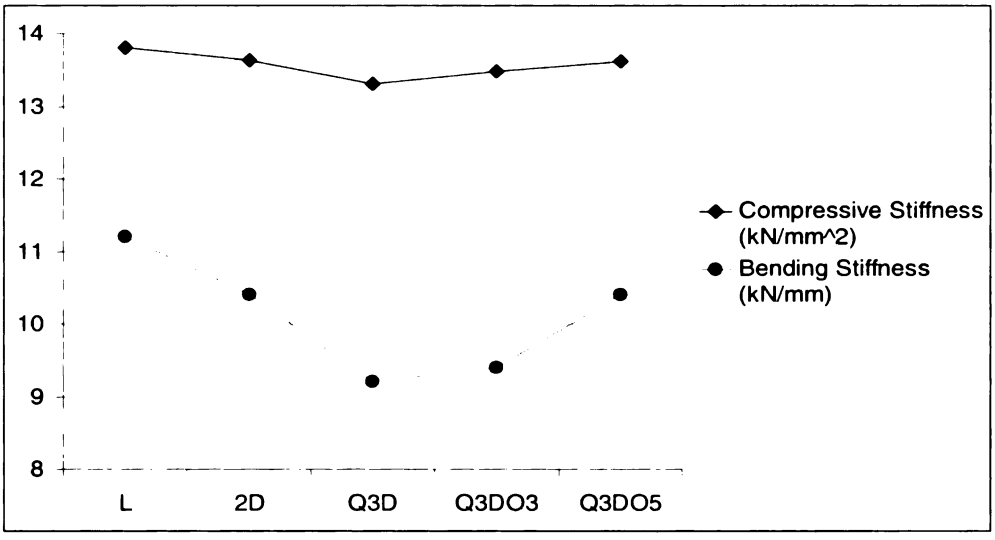

Figure 6.8. Compressive stiffness and bending stiffness comparison

It is seen from the two plots in Figure 6. that the trend in the stiffness measured in both cases is very similar. As expected, L has the highest stiffness value in both cases. Q3D was expected to have the lowest stiffness values as it is two-harness (high frequency of undulation) and quasi-three-dimensionally woven (each undulation goes over two yarn thicknesses). Stiffness of 2D is somewhere in between that of L and Q3D as it has two harness, but the undulation is only one yarn thickness deep. It is seen how, by increasing the harness number of the quasi-three-dimensional weave, the stiffness values get higher. This is because there are now longer lengths to straight unwoven yarns due to the high harness. Q3DO3 and Q3DO5 had increasing stiffness values as compared to Q3D. It is interesting to note that Q3DO5 had stiffness values equal to that of 2D in both cases. This implies that the overall level of undulation in both cases is similar, even though Q3DO5 has the advantage of being three-dimensionally integrated.

6.3.2 Load-Bearing Ability and Residual Properties After Impact

Maximum compressive load-bearing ability was measured for undamaged specimens and also for damaged specimens which had undergone perforation. Figure 6.9 shows the load at which there was the first big breach of structural integrity in the samples (first big drop in load-bearing ability). As was expected, L samples which have their fibers perfectly aligned with the load were able to bear the largest load before failing. Q3DO5 probably performed better than 2D (even though it has a similar undulation) as the inter-layer integration is better in the former. Compressive strength is sensitive to delamination resistance, as failure occurs by micro-buckling of fibers.

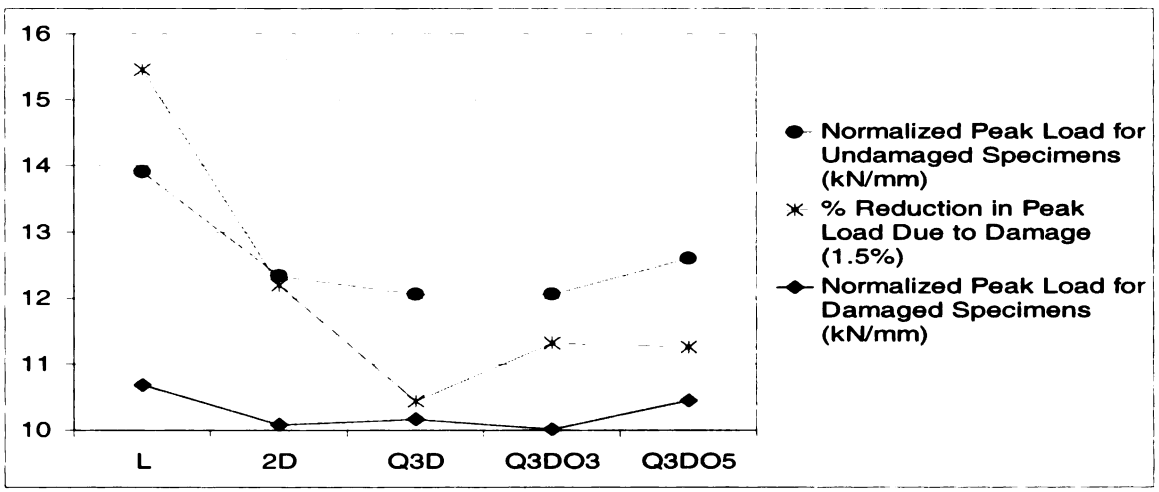

Figure 6.9. Load bearing ability for compression test samples

When damage was introduced into the specimens, the scenario changed. The value of percentage loss of load-bearing ability after damage is a measure of the residual strength in the material and also the materials sensitivity to damage. It can be seen that all quasi-three-dimensional weaves performed better than conventional weaves in residual properties. It should be pointed out that as far as

Q3D and Q3DO3 are concerned, they started off with lower undamaged compressive load values and thus the low percentage loss values might be slightly misleading.

However, Q3DO5 proved itself to be a good configuration again, as it started off with an undamaged load-bearing ability greater than 2D and in this case, the lower percentage loss in load due to damage is truly indicative of an advantage. Laminated (L) samples showed such a big drop in load after impact because impact causes delamination cracks which are unconstrained in L samples. Once these cracks are initiated, failure occurs much easier as each ply is free to separate from the structure and buckle. Similarly for 2D, but to a lesser extent.

6.4 Damage Area and Damage Resistance

6.4.1 Impact Damage

It is understood that primary damage area is of greater consequence to the overall structural integrity of the material than secondary damage area. This is because the former affects the through-thickness strength of the material, while the latter only affects the surface. As was seen in Figure 6.5, all the Quasi-three-dimensional weaves had smaller primary damage areas than the conventional weaves. This is a measure of damage resistance. The consequence of this is clearly seen in the compressive tests where the Quasi-three-dimensional weaves were able to retain more of their initial compressive load-bearing ability. High harness quasi-three-dimensional weaves gained their energy absorption advantage from the secondary fiber straining without risking

through-thickness damage increase to absorb energy. The ability of Quasi-three-dimensional weaves to effectively cut off delamination growth is more clearly seen in the following section.

6.4.2 Compressive Damage

In compressive testing, there were two distinct modes of failure. The first was shear fracture which was seen primarily in L, 2D and Q3DO5 specimens. Here the specimens failed catastrophically and instantaneously with a sudden drop of load down to near zero, without any prior signs of failure. A cross-section of such failure was shown in Figure 5.31. The samples in these cases lost all structural integrity, and sheared into two separate pieces in some cases.

All samples in this damage mode group have something in common. They all have lower delamination resistance than Q3D and Q3DO3. L and 2D by virtue of their not being three-dimensionally integrated and Q3DO5 by virtue of high harness number which maintains larger layers that are not integrated with the neighbouring layers. In these cases, each layer is more free to separate from the structure by buckling and bear the load individually. Once the first layer buckled and failed, it was a 'chain reaction' where the consecutively weakening structure failed catastrophically.

In the Q3D and Q3DO3 sample groups, there was a more encouraging damage mode, seen in a majority of the cases. When the sample lost its structural integrity (first big drop in load), the load did not drop down to near zero, but stopped at an intermediate value and began to pick up again. This can be seen in the load curves in Figure 5.26 and Figure 5.27 of Chapter 5. Figure 5.34

showed the curve of the one specimen that was allowed to flex and fail past the first drop in load. It is seen that failure was not by catastrophic shear. At the point of the first drop in load, many specimens showed audible and load-based signs of impending failure. This can be seen in the figure as the first drop in load at peak load. Once the specimen damaged, the load dropped and it buckled into an 's' shape at the free span in the compression fixture, and the entire cross section bore this buckling load. On further loading the resistance offered by this buckled section increased until it reached a second failure point where the specimen failed by double shear at the support points of the free span. This damage was still only seen on one side of the specimen, with the other side still in this 's' shape.

In these small harness Quasi-three-dimensional cases, when the weakest layer buckled, the three-dimensionally integrated weaves pulled the rest of the cross-section along with it, and so the entire section bore the load collectively without allowing individual layers to fail. Even though both Q3D and Q3DO3 weaves had the lowest undamaged load bearing ability (due to their higher level of undulation), this kind of yielding failure is considered a design advantage as it warns of impending failure and also has some structural integrity remaining after the first loss of strength.

In the shearing-based compression failure mode, a clear frature line due to shear is seen in the specimen along with unbounded internal delamination as seen in Figure 5.30. Internal delamination would not be expected to be high in

shear damage as compared with buckling damage which is sure to induce large-scale internal delamination for L specimens.

Figure 5.35 showed a representative sample of the buckling failure in a Q3D sample. It can be seen that there is wide spread interal delamination, with no clear line of failure like that seen in the compressive failure. It is impressive to see that even though the delaminated region (dark region in figure) was put through an intense local bending, the delamination was contained within the boundaries of the Q3D specimen's unit cell. In the Q3DO3 samples, the delamination spread to two yarns width (which is the length of its unit cell). If it was a conventional sample in this kind of bending, there would have been no bounding control over the extent of spread of this delamination. This, along with lower *primary damage* area in impact tests, shows the ability of Quasi-three-dimensional weaves to control delamination.

CHAPTER 7

Conclusions and Recommendations

7.1 Summary of Testing

a) Thin sample sets of 2mm thickness of laminated (L), two-dimensional (2D) woven, two-harness Quasi-three-dimensional (Q3D) woven, three-harness Quasi-three-dimensional (Q3DO3) with offset woven and five-harness Quasi-three-dimensional (Q3DO5) with offset woven configurations were prepared by hand weaving and cured at elevated temperatures. Impact tests along with high-speed photography were performed on these specimens to measure impact characteristics to study damage behavior. Through-thickness damage (*primary damage*) and rear-layer surface-damage (*secondary damage*) were measured using a light table. From these values, *specific energy absorption (SEA)* was calculated.

b) Thick sample sets of 6mm thickness of the L, 2D and Q3DO5 configurations were also prepared in a similar manner. In addition a modified version of the Q3DO5 weave (designated Q3DO5X) was prepared to isolate the rear-fiber straining phenomenon. They were impact tested to measure energy absorption and verify the *rear-layer fiber straining hypothesis*.

c) Un-impacted and impacted thin specimens of all five configurations were put through in-plane compression tests to measure compressive stiffness and load-bearing ability before and after impact damage. Their damage patterns were studied using a light table.

7.2 Conclusions

From this study, a number of conclusions can be reached:

a) Rear-layer fiber straining was an important energy absorption mechanism in high-harness Quasi-three-dimensional weaves. It allowed thin specimens of them to hold a high load (around peak load) for an extended period of time (corresponding to 1.5 mm deflection in Q3DO3 and 2.5 mm deflection in Q3DO5 specimens), contributing to higher energy absorption.

b) Although rear-layer fiber straining was more valuable in thin specimens where its effect could stand out over the contribution of the fewer other layers, it could be used to an energy absorbing advantage in thick specimens too by increasing the thickness of the rear layers.

c) Three-harness Q3DO3 and five-harness Q3DO5 configurations could match up to energy absorption capabilities of conventional L and 2D configurations for thin specimens due to this secondary fiber straining. In thick specimens, the Q3DO5 was not able to match energy absorption of L due to the smaller prominence of the rear-layer fiber straining over the contribution of the other numerous layers. But it did manage to outperform 2D (6% higher). This was improved in the Q3DO5 X specimen which was able to match energy absorption of the laminated specimens too, showing that it was possible to get the same advantage in thicker specimens. This configuration absorbed 8% higher impact energy than the regular Th Q3DO5 configuration purely by the redistribution of fiber content to thicken the rear layers.

d) Quasi-three-dimensional weaves showed improved delamination control over conventional configurations. Their primary damage areas in all cases were lower than those of conventional weaves (14%-20% lower). Compression tests showed the ability of the Q3D weave to contain damage within one unit cell.

e) Accounting for both, energy absorption and damage area, *specific energy absorption (SEA)* was higher for all Quasi-three-dimensional weaves as compared to conventional weaves (15%-30% higher than the conventional average).

f) All Quasi-three-dimensional weaves showed a lower percentage loss in strength (15.7%-17%) due to impact damage than conventional weaves (18.3%-23.3%) in compression tests. This demonstrated higher damage control and higher residual strength after impact.

g) Low harness Quasi-three-dimensional weaves (Q3D and Q3DO3) showed favorable yielding kind of bending failure in compression instead of catastrophic shear as seen in other specimens. This kind of failure mode warned of impending failure and retained some strength even after the first breach in structural integrity. This might prove useful in practice as it allows for timely repair.

h) Five-harness Q3DO5 was found to be the most favorable configuration as it matched the compressive and bending stiffness of conventional 2D weave, showed the highest energy absorption, highest *specific energy absorption*, low *primary damage* area and low percentage loss in load-bearing ability after impact as compared with the other configurations. This would also be the easiest of the

Quasi-three-dimensional weaves to produce due to less frequent interlocking of fibers.

7.3 Recommendations for Future Work

Based on the lessons learnt from this study, the following recommendations are offered for future work on this topic:

a) Thickness control dams that were used in the curing of the thick specimens proved invaluable to maintaining perfect flatness and repeatability of thickness in those specimens. This reduced the percentage deviations in the measured quantities and removed any added influence of thickness difference between samples. This should be used in all sample curing henceforth.

b) The thin samples were produced with a very high fiber volume fraction (~68%) which caused the specimens to be brittle resulting in very small damage areas in all cases. This made differentiating results harder. Future studies should use the thickness control dams of a dimension such that only a little resin is removed from the prepreg during curing. This would assure that it was well compacted, but also provided a higher matrix fraction, yielding a less stiff and brittle sample.

c) Another factor leading to small damage areas was the use of very thin tows in the weaving process. The thickness of the prepreg used in future studies should be increased. This would help to exaggerate the delamination effect to better study the phenomenon. It should be noted that in any real-life application, the opposite would be advantageous, as delamination is to be minimized.

d) High-speed camera photography should be done at a minimum of 4000 frames per second to ensure sufficiently accurate recording of the damage process. In this study, some cases were run at a lower shutter speed leading to gaps of unknown activity in the damage process. Sufficient lighting should be provided to yield high contrast pictures.

e) Loading edges in compression test samples should be milled flat and parallel (although the pin joint in the fixture will take up small non-parallelisms). In this study, loading edges were hand polished on a flat abrasive. A few samples had to be rejected due to local brooming damage at the loading surfaces due to irregularities in these surfaces.

f) Transparent samples should be produced of the different weave configurations so that along with a high-speed camera, the internal damage sequence could be more thoroughly studied.

APPENDICES

APPENDIX A

Pictures of Impacted Specimens (backlit and rear surface)

NOTE: Nomenclature on sample is to be ignored

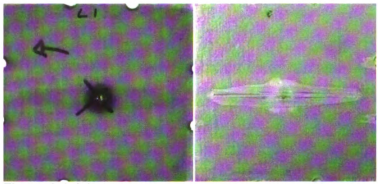

Figure A.1. L1

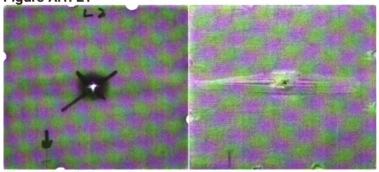

Figure A.2. L2

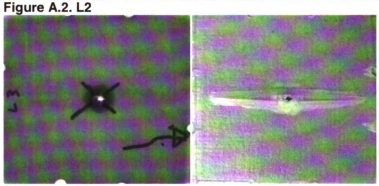

Figure A.3. L3

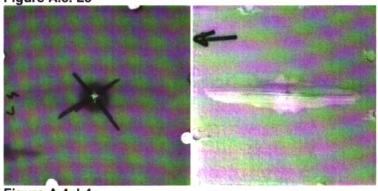

Figure A.4. L4

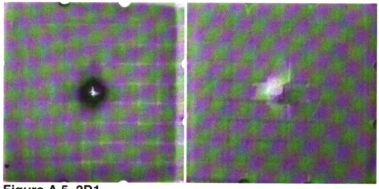

Figure A.5. 2D1

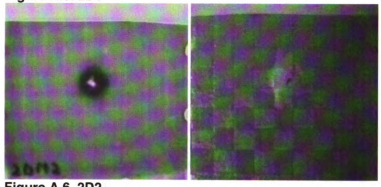

Figure A.6. 2D2

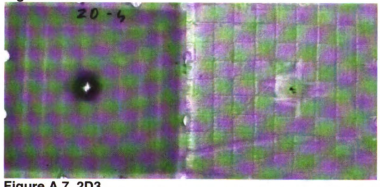

Figure A.7. 2D3

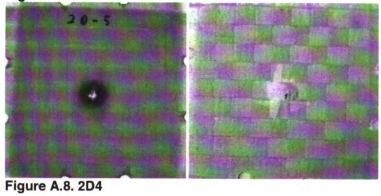

Figure A.8. 2D4

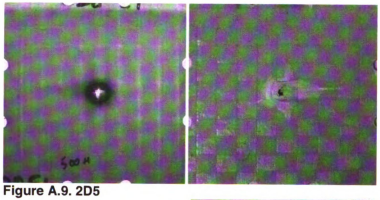

Figure A.9. 2D5

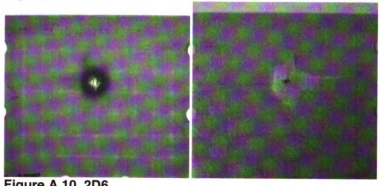

Figure A.10. 2D6

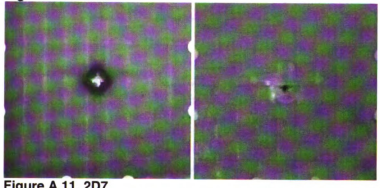

Figure A.11. 2D7

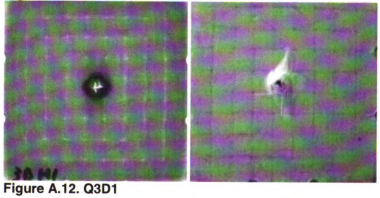

Figure A.12. Q3D1

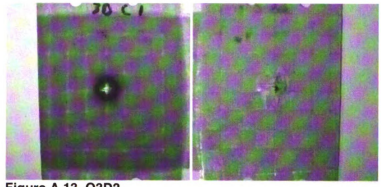

Figure A.13. Q3D2

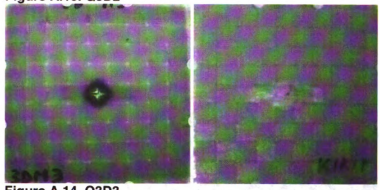

Figure A.14. Q3D3

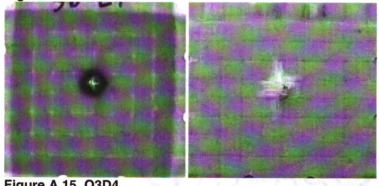

Figure A.15. Q3D4

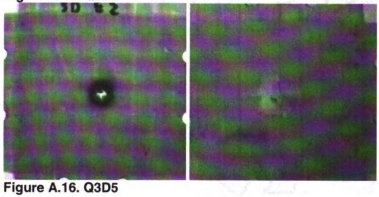

Figure A.16. Q3D5

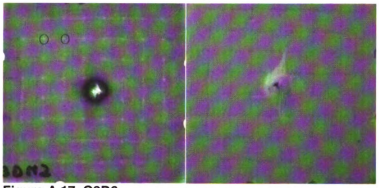

Figure A.17. Q3D6

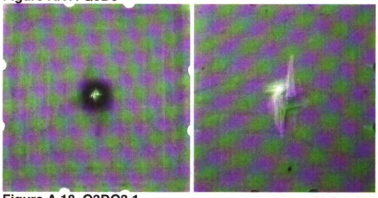

Figure A.18. Q3DO3 1

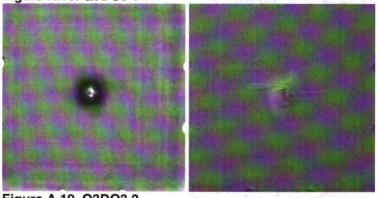

Figure A.19. Q3DO3 2

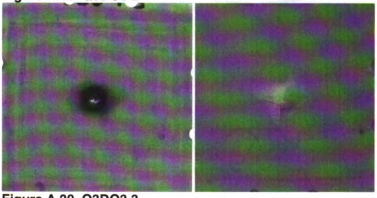

Figure A.20. Q3DO3 3

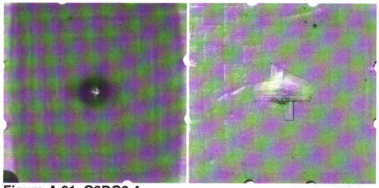

Figure A.21. Q3DO3 4

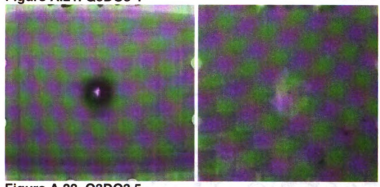

Figure A.22. Q3DO3 5

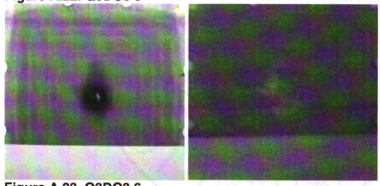

Figure A.23. Q3DO3 6

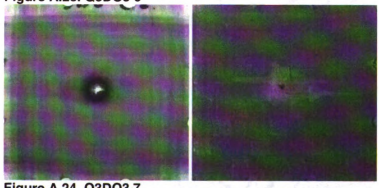

Figure A.24. Q3DO3 7

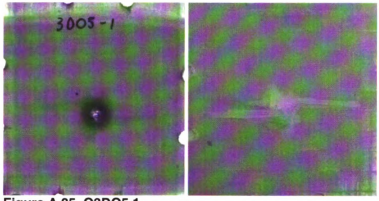

Figure A.25. Q3DO5 1

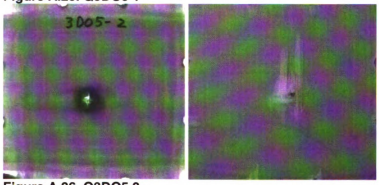

Figure A.26. Q3DO5 2

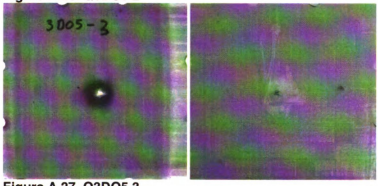

Figure A.27. Q3DO5 3

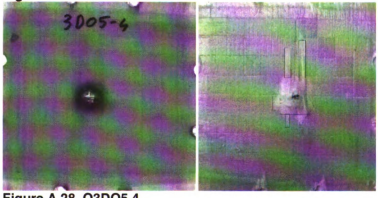

Figure A.28. Q3DO5 4

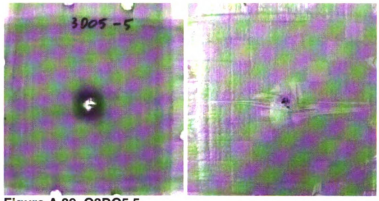

Figure A.29. Q3DO5 5

APPENDIX B

Pictures of Compression Test Specimen (backlit)

NOTE: Nomenclature used on the samples is to be ignored.

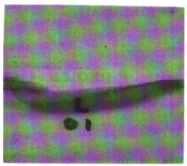

Figure B.1. L1

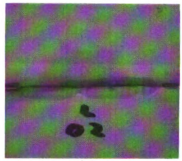

L2

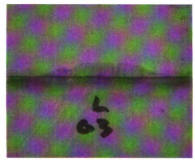

L3

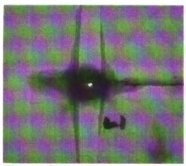

Figure B.2. dL1

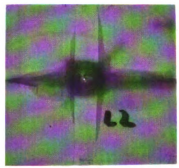

dL2

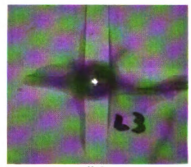

dL3

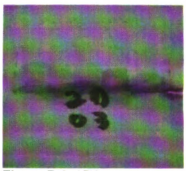

Figure B.3. 2D1

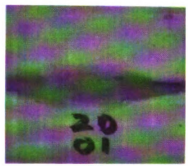

2D2

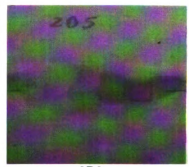

2D3

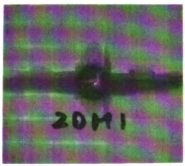

Figure B.4. d2D1

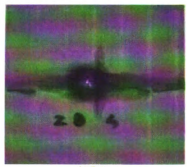

d2D2

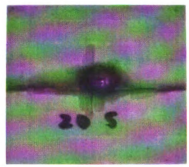

d2D3

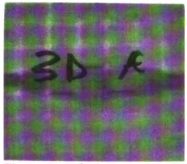

Figure B.5. Q3D1

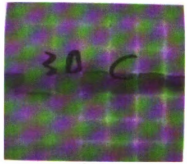

Q3D2

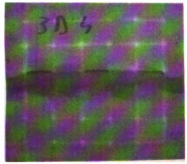

Q3D3

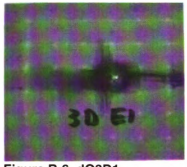

Figure B.6. dQ3D1

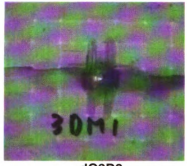

dQ3D2

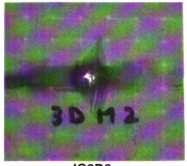

dQ3D3

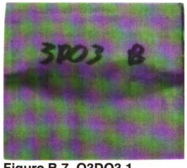

Figure B.7. Q3DO3 1

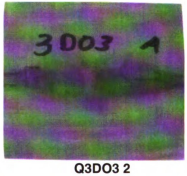

Q3DO3 2

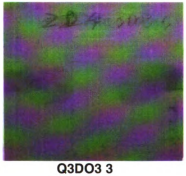

Q3DO3 3

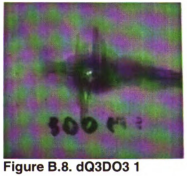

Figure B.8. dQ3DO3 1

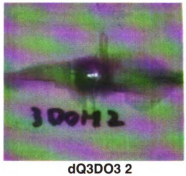

dQ3DO3 2

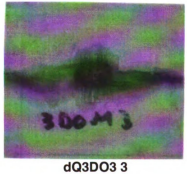

dQ3DO3 3

Figure B.9. Q3DO5 1

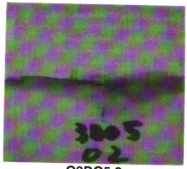

Q3DO5 2

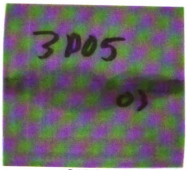

Q3DO5 3

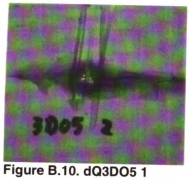

Figure B.10. dQ3DO5 1

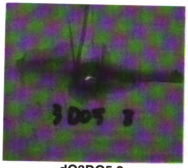

dQ3DO5 2

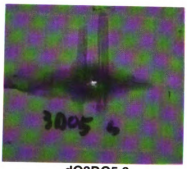

dQ3DO5 3

REFERENCES

REFERENCES

1. D. Liu. "Delamination Resistance in Stitched and Unstitched Composite Plates Subjected to Impact Loading," *Journal of Reinforced Plastics and Composites,* 1990; 9; 59-69

2. B.M. Icten, D. Liu. "Effects of Composite Cell Size and Weaving Angle on Impact Resistance"

3. A.L. Pilchak, T, Uchiyama, D.Liu. "Low Velocity Impact Response of Small-Angle Laminated Composites," *AIAA Journal,* Vol. 44; No.12; December 2006, 3080-3087

4. S. Sanchez-Saez, E. Barbero, R. Zaera, C. Navarro. "Compression After Impact of Thin Composite Laminates," *Composites Science and Technology* 65 (2005); 1911-1919

5. G. Coppens, " Effect of Three-Dimensional Geometry on Penetration and Perforation Resistance," A Thesis, Department of Mechanical Engineering, Michigan State University, 2004

6. C Atas, D. Liu, "Impact Response of Woven Composites with Small Weaving Angles," *International Journal of Impact Engineering* (2007), 1-23

7. Tien-Wei Shyr, Yu-Hao Pan. "Impact Resistance and Damage Characteristics of Composite Laminates," *Composite Structures* 62 (2003); 193-203

8. F.K. Ko, "Textile Preforms for Carbon-Carbon Composites," National Aeronautics and Space Administration, *Carbon--Carbon Materials and Composites (USA),* 1992, pp. 71-104, 1992

9. M.H. Mohamed, A.E. Bogdanovich, Dr. Habil. Sc. Ing., L.C. Dickinson, J.N. Singletary, R.B. Lienhart, "A New Generation of 3D Woven Fabric Preforms and Composites," *Sampe Journal,* Vol. 37, No. 3, May/June 2001, 8-17

10. X. Zhang, L. Hounslow, M. Grassi, " Improvement of Low Velocity Impact and Compression-After-Impact Performance by Z-Fiber Pinning," *Composites Science and Technology,* 66 (2006): 2785-2794

11. B.A. Cheeseman, T.A. Bogetti. "Ballistic Impact into Fabric and Compliant Composite Laminates," *Composite Structures* 61 (2003); 161-173

12. L.A. Ruhala, R.S. Engel, " A Study of the Impact Resistance of Fiber Reinforced Composite Laminated Plates Due to Various Relative Fiber

Contents and Densities," *Journal of Thermoplastic Composite Materials* 1999, 12; 227-239

13. B.A. Cheeseman, C.F. Yen, B.R. Scott, B. Powers, T.A. Bogetti, B. LaMattina, Y. Duan, M. Keefe, Y. Miao, Y. Wang, "From Filaments to Fabric Packs-Simulating the Performance of Textile Protection Systems"

14. Y.Q. Wang, A.S.D. Wang, "Spatial Distribution of Yarns and Mechanical Properties in 3D Braided Tubular Composites," *Applied Composite Materials* 4: 121-132. 1997

15. Zheng-Ming Huang, "Efficient Approach to the Structure –Property Relationship of Woven and Braided Fabric –Reinforced Composites up to Failure," *Journal of Reinforced Plastics and Composites* 2005; 24; 1289-1309

16. Y. Wang, D. Zhao, "Effect of Fabric Structures on the Mechanical Properties of 3-D Textile Composites," *Journal of Industrial Textiles,* Vol. 35, No. 3; January 2006, 239-256

17. H.L. Yi, X. Ding, "Conventional Approach on Manufacturing 3D Woven Preforms used for Composites," *Journal of Industrial Textiles,* Vol. 34, No. 1-July 2004, 39-50

18. M.V. Hosur, M. Adya, J. Alexander, S. Jeelani, U. Vaidya, A. Mayer, " Studies on Impact Damage Resistance of Affordable Stitched Woven Carbon/Epoxy Composite Laminates," *Journal of Reinforced Plastics and Composites* 2003; 22; 927-952

19. A.P. Mouritz, K.H. Leong, I. Herszberg, " A Review of the Effects of Stitching on the In-Plane Mechanical Properties of Fiber Reinforced Polymer Composites," *Composites Part A **28A** (1997) 979-991*

20. S. Rudov-Clark, A.P. Mouritz, L. Lee, M.K. Bannister, "Fiber Damage in the Manufacture of Advanced Three Dimensional Woven Composites," *Composites:* Part A 34 (2003); 963-970

21. B. Lee, K.H. Leong, I. Herszberg,"Effect of Weaving on the Tensile Properties of Carbon Fiber Tows and Woven Composites," *Journal of Reinforced Plastics and Composites* 2001; 20; 652-670

22. D. Liu, B.B. Raju, X Dang, " Size Effect on Impact Response of Composite Laminates," *International Journal of Impact Engineering* Vol. 21; No. 10; 837-854; 1998

23. N.K. Naik, S.V. Borade, H. Arya, M. Sailendra, S.V. Prabhu, "Experimental Studies on Impact Behavior of Woven Fabric Composites: Effect of Impact

Parameters," *Journal of Reinforced Plastics and Composites* 2002; 21; 1347-1362

24. C. Ulven, U.K. Vaidhya, M.V. Hosur, " Effect of Projectile Shape During Ballistic Perforation of VARTM Carbon/Epoxy Composite Panels," *Composite Structures* 61 (2003) 143-150

25. Y.P. Siow and V.P.W. Shim, " An Experimental Study of Low Velocity Impact Damage in Woven Fiber Composites," *Journal of Composite Materials* 1998; Vol. 32, No. 12; 1178-1202

26. D Liu, L.S. Lillycrop, L.E. Malvern, C.T. Sun, " the Evaluation of Delamination-An Edge Replication Study," *Experimental Techniques (1987);* 20-25

27. O.A. Khondker, K.H. Leong, I. Herszberg, H. Hamada, "Impact and Compression-After-Impact Performance of Weft Knitted Glass Textile Composites," *Composites* : Part A 36 (2005) 638-648

28. Standard Test Method for Measuring the Damage Resistance of a Fiber-Reinforced Polymer Matrix Composite to a Drop-Weight Impact Event[1], D 7136/D7136M- 05$^{\varepsilon 1}$

29. B.L. Lee, T.F. Walsh, S.T. Won, H.M. Patts, J.W. Song, A.H. Mayer, "Penetration Failure Mechanisms of Armor-Grade Fiber Composites under Impact," *Journal of Composite Materials,* Vol. 35, No. 18/2001, 1605-1633

30. Standard Test Method for Compressive Residual Strength Properties of Damaged Polymer Matrix Composite Plates, ASTM D 7137/D7137M-05$^{\varepsilon 1}$